

1 Single-trial characterization of neural rhythms: potential and challenges

2
3 Julian Q. Kosciessa^{1,2,*}, Thomas H. Grandy², Douglas D. Garrett^{1,2}, Markus Werkle-
4 Bergner^{2,*}

5
6 ¹Max Planck UCL Centre for Computational Psychiatry and Ageing Research,
7 Berlin/London; ²Center for Lifespan Psychology, Max Planck Institute for Human
8 Development, Lentzeallee 94, 14195 Berlin, Germany.

9
10 * Corresponding authors:

11 kosciessa@mpib-berlin.mpg.de; werkle@mpib-berlin.mpg.de

12
13 Abstract

14
15 The average power of rhythmic neural responses as captured by MEG/EEG/LFP recordings is
16 a prevalent index of human brain function. Increasing evidence questions the utility of trial-
17 /group averaged power estimates, as seemingly sustained activity patterns may be brought
18 about by time-varying transient signals in each single trial. Hence, it is crucial to accurately
19 describe the duration and power of rhythmic and arrhythmic neural responses on the single
20 trial-level. However, it is less clear how well this can be achieved in empirical MEG/EEG/LFP
21 recordings. Here, we extend an existing rhythm detection algorithm (extended **B**etter
22 **O**SCillation detection: “eBOSC”; cf. Whitten et al., 2011) to systematically investigate
23 boundary conditions for estimating neural rhythms at the single-trial level. Using simulations
24 as well as resting and task-based EEG recordings from a micro-longitudinal assessment, we
25 show that alpha rhythms can be successfully captured in single trials with high specificity, but
26 that the quality of single-trial estimates varies greatly between subjects. Importantly, our
27 analyses suggest that rhythmic estimates are reliable within-subject markers, but may not be
28 consistently valid descriptors of the individual rhythmic process. Finally, we highlight the
29 utility and potential of rhythm detection with multiple proof-of-concept examples, and discuss
30 various implications for single-trial analyses of neural rhythms in electrophysiological
31 recordings.

32
33 Keywords: rhythm detection; abundance; alpha power; inter-individual differences; single-trial
34 estimates

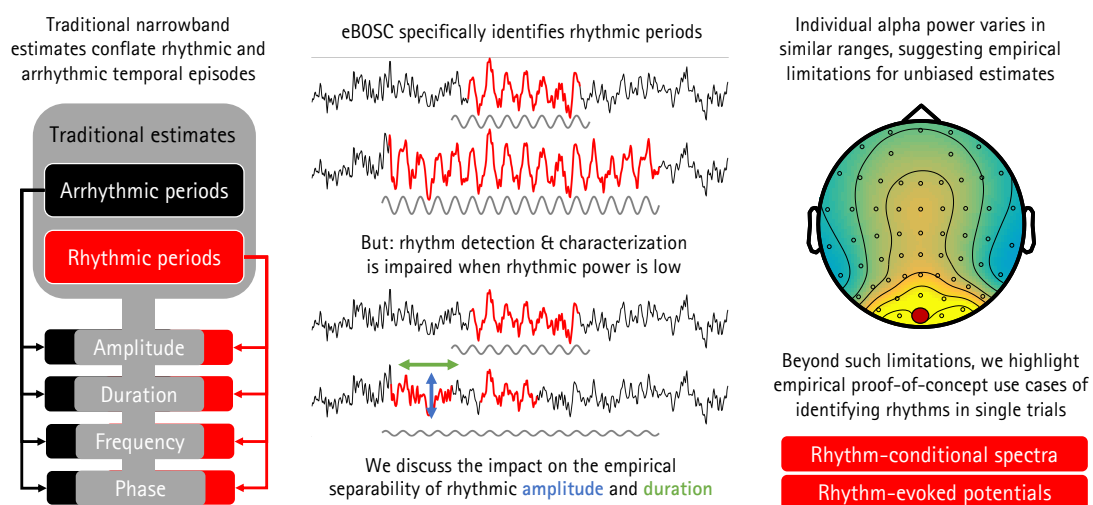
RUNNING HEAD: SINGLE-TRIAL CHARACTERIZATION OF NEURAL RHYTHMS

35 Highlights

- 36 • Traditional narrow-band rhythm metrics conflate the power and duration of rhythmic
37 and arrhythmic periods.
- 38 • We extend a state-of-the-art rhythm detection method (eBOSSC) to derive rhythmic
39 episodes in single trials that can disambiguate rhythmic and arrhythmic periods.
- 40 • Simulations indicate that this can be done with high specificity given sufficient rhythmic
41 power, but with strongly impaired sensitivity when rhythmic power is low.
- 42 • Empirically, surface EEG recordings exhibit stable inter-individual differences in α -
43 rhythmicity in ranges where simulations suggest a gradual bias, leading to high
44 collinearity between narrow-band and rhythm-specific estimates.
- 45 • Beyond these limitations, we highlight multiple empirical proof-of-concept benefits of
46 characterizing rhythmic episodes in single trials.

47

eBOSSC disambiguates rhythmic and arrhythmic periods in single trials



48

RUNNING HEAD: SINGLE-TRIAL CHARACTERIZATION OF NEURAL RHYTHMS

49 1.1 Towards a single-trial characterization of neural rhythms 50

51 Episodes of rhythmic neural activity in electrophysiological recordings are of prime
52 interest for research on neural representations and computations across multiple scales of
53 measurement (e.g. Buzsáki, 2006; Wang, 2010). At the macroscopic level, the study of
54 rhythmic neural signals has a long heritage, dating back to Hans Berger's classic investigations
55 into the Alpha rhythm (Berger, 1938). Since then, advances in recording and processing
56 techniques have facilitated large-scale spectral analysis schemes (e.g. Gross, 2014) that were
57 not available to the pioneers of electrophysiological research, who often depended on the
58 manual analysis of single time series to indicate the presence and magnitude of rhythmic events.
59 Interestingly, improvements in analytic methods still do not capture all of the information that
60 can be extracted by manual inspection. For example, current analysis techniques are largely
61 naïve to the specific temporal presence of rhythms in the continuous recordings, as they often
62 employ windowing of condition- or group-based averages to extract putative rhythm-related
63 characteristics (Cohen, 2014). However, the underlying assumption of stationary, sustained
64 rhythms within the temporal window of interest might not consistently be met (Jones, 2016;
65 Stokes & Spaak, 2016), thus challenging the appropriateness of the averaging model (i.e., the
66 ergodicity assumption (Molenaar & Campbell, 2009)). Furthermore, in certain situations,
67 single-trial characterizations become necessary to derive unbiased individual estimates of
68 neural rhythms (Cohen, 2017). For example, this issue becomes important when asking whether
69 rhythms appear in transient or in sustained form (van Ede, Quinn, Woolrich, & Nobre, 2018),
70 or when only single-shot acquisitions are feasible (i.e., resting state or sleep recordings).

71 72 1.2 Duration as a powerful index of rhythmicity 73

74 The presence of rhythmicity is a necessary prerequisite for the accurate interpretation
75 of measures of amplitude, power, and phase (Aru et al., 2015; Jones, 2016;
76 Muthukumaraswamy & Singh, 2011). This is exemplified by the bias that arrhythmic periods
77 exert on rhythmic power estimates. Most current time-frequency decomposition methods of
78 neurophysiological signals (such as the electroencephalogram (EEG)) are based on the Fourier
79 transform (Gross, 2014). Following Parseval's theorem (e.g. Hansen, 2014), the Fast Fourier
80 Transform (FFT) decomposes an arbitrary time series into a sum of sinusoids at different
81 frequencies. Importantly, FFT-derived power estimates do not differentiate between high
82 amplitude transients and low amplitude sustained signals. In the case of FFT power, this is a

RUNNING HEAD: SINGLE-TRIAL CHARACTERIZATION OF NEURAL RHYTHMS

83 direct result of the violated assumption of stationarity in the presence of a transient signal.
84 Short-time FFT and wavelet techniques alleviate (but do not eliminate) this problem by
85 analyzing shorter epochs, during which stationarity is more likely to be obtained. However,
86 whenever spectral power is averaged across these episodes, both high-amplitude rhythmic and
87 low-amplitude arrhythmic signal components may once again become intermixed. In the
88 presence of arrhythmic content (often referred to as the “signal background,” or “noise”), this
89 results in a reduced amplitude estimate of the underlying rhythm, the extent of which relates to
90 the duration of the rhythmic episode relative to the length of the analyzed segment (which we
91 will refer to as ‘abundance’) (see Figure 1A). Therefore, integration across epochs that contain
92 a mixture of rhythmic and arrhythmic signals results in an inherent ambiguity between the
93 strength of the rhythmic activity (as indexed by power/amplitude) and its duration (as indexed
94 by the abundance of the rhythmic episode within the segment) (see Figure 3B).

95 Crucially, the strength and duration of rhythmic activity theoretically differ in their
96 neurophysiological interpretation. Rhythmic power most readily indexes the magnitude of
97 synchronized changes in membrane potentials within a network (Buzsáki, Anastassiou, &
98 Koch, 2012), and is thus related to the size of the participating neural population. The duration
99 of a rhythmic episode, by contrast, tracks how long population synchrony is upheld. Notably,
100 measures of rhythm duration have recently gained interest as they may provide additional
101 information regarding the biophysical mechanisms that give rise to the recorded signals
102 (Peterson & Voytek, 2017; Sherman et al., 2016), for example, by differentiating between
103 transient and sustained rhythmic events (van Ede et al., 2018).

104

105 1.3. Single-trial rhythm detection as a methodological challenge

106

107 In general, the accurate estimation of process parameters depends on a sufficiently strong
108 signal in the neurophysiological recordings under investigation. Especially for scalp-level
109 M/EEG recordings it remains elusive whether neural rhythms are sufficiently strong to be
110 clearly detected in single trials. Here, a large neural population has to be synchronously active
111 to give rise to potentials that are visible at the scalp surface. This problem intensifies further by
112 signal attenuation through the skull (in the case of EEG) and the superposition of signals from
113 diverse sources of no interest both in- and outside the brain (Lopez da Silva, 2018). In sum,
114 these considerations lead to the proposal that the signal-to-noise ratio (SNR), here operationally
115 defined as the ratio of rhythmic to arrhythmic variance, may fundamentally constrain the
116 accurate characterization of single-trial rhythms.

RUNNING HEAD: SINGLE-TRIAL CHARACTERIZATION OF NEURAL RHYTHMS

117 Following those considerations, we set out to answer the following hypotheses and
118 questions: (1) A precise differentiation between rhythmic and arrhythmic timepoints can
119 disambiguate the strength and the duration of rhythmicity. (2) To what extent does the single-
120 trial rhythm representation in empirical data allow for an accurate estimation of rhythmic
121 strength and duration in the face of variations in the signal-to-noise ratio of rhythmicity? (3)
122 What are the empirical benefits of separating rhythmic (and arrhythmic) duration and power?

123 Recently, different methods have been proposed to characterize rhythmicity at the single-
124 trial level: the power-based Better OSCillation Detection (BOSC; Caplan, Madsen,
125 Raghavachari, & Kahana, 2001; Whitten, Hughes, Dickson, & Caplan, 2011) and the phase-
126 based lagged coherence index (Fransen, van Ede, & Maris, 2015). Notably, both proposed
127 algorithms make different assumptions regarding the definition of rhythmicity: BOSC assumes
128 that rhythms are defined as spectral peaks that are superimposed on an arrhythmic 1/f
129 background, whereas lagged coherence defines rhythms based on the predictability of phase
130 estimates at a temporal lag that is defined by the rhythm's period.

131 Here, we extend the BOSC method (i.e., extended BOSC; eBOSC) to derive rhythmic
132 temporal episodes that can be used to further characterize rhythmicity. Using simulations, we
133 derive rhythm detection benchmarks and probe the boundary conditions for unbiased rhythm
134 indices. Furthermore, we apply the novel eBOSC algorithm to resting- and task-state data from
135 a micro-longitudinal dataset to systematically investigate the feasibility to derive reliable and
136 valid indices of neural rhythmicity from single-trial scalp EEG data. We calculate lagged
137 coherence during the resting state to probe the inter-individual convergence between rhythm
138 definitions. Finally, we showcase eBOSC's ability to characterize rhythmic and arrhythmic
139 content. We focus on alpha rhythms (~8-15 Hz; defined here based on individual FFT-peaks)
140 due to (a) their high amplitude in human EEG recordings, (b) the previous focus on the alpha
141 band in the rhythm detection literature (Caplan, Bottomley, Kang, & Dixon, 2015; Fransen et
142 al., 2015; Whitten et al., 2011), and (c) their importance for human cognition (Grandy, Werkle-
143 Bergner, Chicherio, Lövdén, et al., 2013a; Klimesch, 2012; Sadaghiani & Kleinschmidt, 2016).
144 We present examples beyond the alpha range to highlight the ability to apply eBOSC in
145 multiple, diverse frequency ranges.

146

147 2. Methods

148

149 2.1 Study design

150

RUNNING HEAD: SINGLE-TRIAL CHARACTERIZATION OF NEURAL RHYTHMS

151 Resting state and task data were collected in the context of a larger assessment,
152 consisting of eight sessions in which an adapted Sternberg short-term memory task (Sternberg,
153 1966) and three additional cognitive tasks were repeatedly administered. Resting state data are
154 from the first session, task data are from sessions one, seven and eight, during which EEG data
155 were acquired. Sessions one through seven were completed on consecutive days (excluding
156 Sundays) with session seven completed seven days after session one by all but one participant
157 (eight days due to a two-day break). Session eight was conducted approximately one week after
158 session seven ($M = 7.3$ days, $SD = 1.4$) to estimate the stability of the behavioral practice
159 effects. The reported EEG sessions lasted approximately three and a half to four hours,
160 including approximately one and a half hours of EEG preparation. For further details on the
161 study protocol and results of the behavioural tasks see (Grandy, Lindenberger, & Werkle-
162 Bergner, 2017).

163

164 2.2 Participants

165

166 The sample contained 32 young adults (mean age = 23.3 years, $SD = 2.0$, range 19.6 to
167 26.8 years; 17 women; 28 university students) recruited from the participant database of the
168 Max Planck Institute for Human Development, Berlin, Germany (MPIB). Participants were
169 right-handed, as assessed with a modified version of the Edinburgh Handedness Inventory
170 (Oldfield, 1971), and had normal or corrected-to-normal vision, as assessed with the Freiburg
171 Visual Acuity test (Bach, 1996; 2007). Participants reported to be in good health with no known
172 history of neurological or psychiatric incidences and were paid for their participation (8.08 €
173 per hour, 25.00 € for completing the study within 16 days, and a performance-dependent bonus
174 of 28.00 €; see below). All participants gave written informed consent according to the
175 institutional guidelines of the ethics committee of the MPIB, which approved the study.

176

177 2.3 Procedure

178

179 Participants were seated at a distance of 80 cm in front of a 60 Hz LCD monitor in an
180 acoustically and electrically shielded chamber. A resting state assessment was conducted prior
181 to the initial performance of the adapted Sternberg task. Two resting state periods were used:
182 the first encompassed a duration of two minutes of continuous eyes open (EO1) and eyes closed
183 (EC1) periods, respectively; the second resting state was comprised of two 80 second runs,

RUNNING HEAD: SINGLE-TRIAL CHARACTERIZATION OF NEURAL RHYTHMS

184 totalling 16 repetitions of 5 seconds interleaved eyes open (EO2) – eyes closed (EC2) periods.
185 An auditory beep indicated to the subjects when to open and close their eyes.

186 Following the resting assessments, participants performed an adapted version of the
187 Sternberg task. Digits were presented in white on a black background and subtended $\sim 2.5^\circ$ of
188 visual angle in the vertical and $\sim 1.8^\circ$ of visual angle in the horizontal direction. Stimulus
189 presentation and recording of behavioral responses were controlled with E-Prime 2.0
190 (Psychology Software Tools, Inc., Pittsburgh, PA, USA). The task design followed the original
191 report (Sternberg, 1966). Participants started each trial by pressing the left and right response
192 key with their respective index fingers to ensure correct finger placement and to enable fast
193 responding. An instruction to blink was given, followed by the sequential presentation of 2, 4
194 or 6 digits from zero to nine. On each trial, the memory set size (i.e., load) varied randomly
195 between trials, and participants were not informed about the upcoming condition. Also, the
196 single digits constituting a given memory set were randomly selected in each trial. Each
197 stimulus was presented for 200 ms, followed by a fixed 1000 ms blank inter-stimulus interval
198 (ISI). The offset of the last stimulus coincided with the onset of a 3000 ms blank retention
199 interval, which concluded with the presentation of a probe item that was either contained in the
200 presented stimulus set (*positive probe*) or not (*negative probe*). Probe presentation lasted 200
201 ms, followed by a blank screen for 2000 ms, during which the participant's response was
202 recorded. A beep tone indicated the end of the trial. The task lasted about 50 minutes.

203 For each combination of load x probe type, 31 trials were conducted, cumulating in 186
204 trials per session. Combinations were randomly distributed across four blocks (block one: 48
205 trials; blocks two through four: 46 trials). Summary feedback of the overall mean RT and
206 accuracy within the current session was shown at the end of each block. At the beginning of
207 session one, 24 practice trials were conducted to familiarize participants with the varying set
208 sizes and probe types. To sustain high motivation throughout the study, participants were paid
209 a 28 € bonus if their current session's mean RT was faster or equal to the overall mean RT
210 during the preceding session, while sustaining accuracy above 90%. Only correct trials were
211 included in the analyses.

212

213 2.4 EEG recordings and pre-processing

214

215 EEG was continuously recorded from 64 Ag/AgCl electrodes using BrainAmp
216 amplifiers (Brain Products GmbH, Gilching, Germany). Sixty scalp electrodes were arranged
217 within an elastic cap (EASYCAP GmbH, Herrsching, Germany) according to the 10% system

RUNNING HEAD: SINGLE-TRIAL CHARACTERIZATION OF NEURAL RHYTHMS

218 (cf. Oostenveld, Fries, Maris, & Schoffelen, 2011) with the ground placed at AFz. To monitor
219 eye movements, two electrodes were placed on the outer canthi (horizontal EOG) and one
220 electrode below the left eye (vertical EOG). During recording, all electrodes were referenced
221 to the right mastoid electrode, while the left mastoid electrode was recorded as an additional
222 channel. Prior to recording, electrode impedances were retained below 5 k Ω . Online, signals
223 were recorded with an analog pass-band of 0.1 to 250 Hz and digitized at a sampling rate of 1
224 kHz.

225 Preprocessing and analysis of EEG data were conducted with the FieldTrip toolbox
226 (Oostenveld et al., 2011) and using custom-written MATLAB (The MathWorks Inc., Natick,
227 MA, USA) code. Offline, EEG data were filtered using a 4th order Butterworth filter with a
228 pass-band of 0.5 to 100 Hz, and were linearly detrended. Resting data with interleaved eye
229 closure were epoched relative to the auditory cue to open and close the eyes. An epoch of -2 s
230 to +3 s relative to on- and offsets was chosen to include padding for the analysis. During the
231 eBOSC procedure, three seconds of signal were removed from both edges (see below), resulting
232 in an effective epoch of 4 s duration that excludes evoked components following the cue onset.
233 Continuous eyes open/closed recordings were segmented to the cue on- and offset. For the
234 interleaved data, the first and last trial for each condition were removed, resulting in an effective
235 trial number of 14 trials per condition. For the task data, we analyzed two intervals: an extended
236 interval to assess the overall dynamics of detected rhythmicity and a shorter interval that
237 focused on the retention period. Unless otherwise noted, we refer to the extended interval when
238 presenting task data. For the extended segments, task data were segmented to 21 s epochs
239 ranging from -9 s to +12 s with regard to the onset of the 3 s retention interval for analyses
240 including peri-retention data. For analyses including only the retention phase, data were
241 segmented to -2 s to +3 s around the retention interval. Note that for all analyses, 3 s of signal
242 were removed on each side of the signal during eBOSC detection, effectively removing the
243 evoked cue activity (2 s to account for edge artifacts following wavelet-transformation and 1 s
244 to account for eBOSC's duration threshold, see section 2.6), except during the extended task
245 interval. Hence, detected segments were restricted to occur from 1s after period onset until
246 period offset, thereby excluding evoked signals. Blink, movement and heart-beat artifacts were
247 identified using Independent Component Analysis (ICA; Bell & Sejnowski, 1995) and removed
248 from the signal. Subsequently, data were downsampled to 250 Hz and all channels were re-
249 referenced to mathematically averaged mastoids. Artifact-contaminated channels (determined
250 across epochs) were automatically detected (a) using the FASTER algorithm (Nolan, Whelan,
251 & Reilly, 2010) and (b) by detecting outliers exceeding three standard deviations of the kurtosis

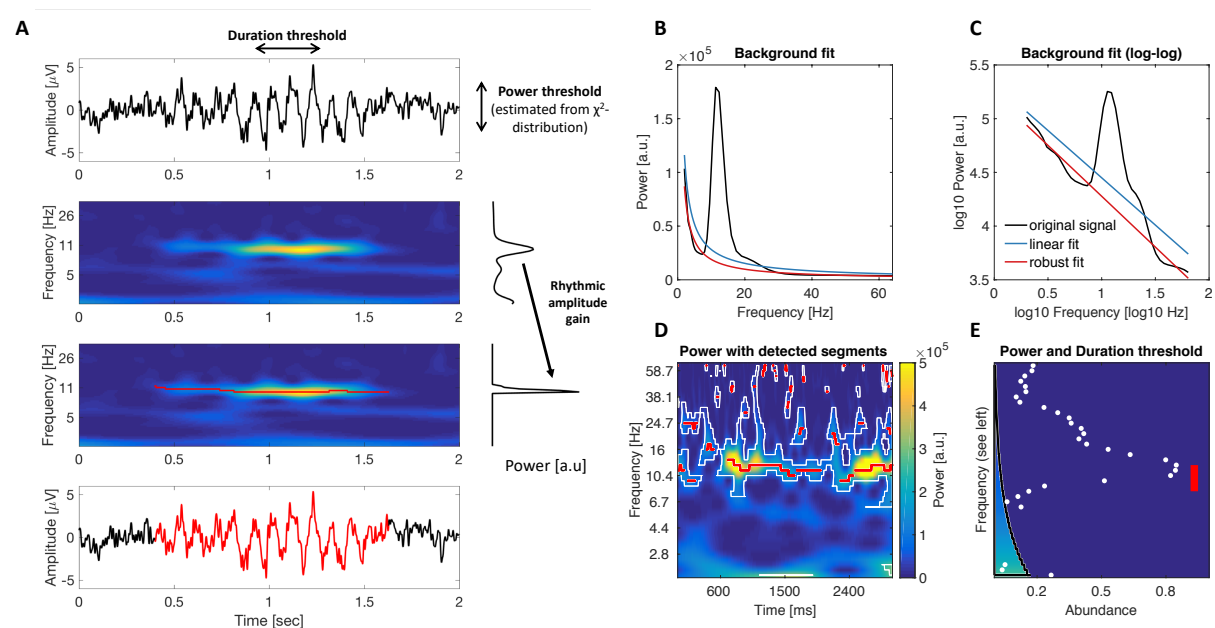
RUNNING HEAD: SINGLE-TRIAL CHARACTERIZATION OF NEURAL RHYTHMS

252 of the distribution of power values in each epoch within low (0.2-2 Hz) or high (30-100 Hz)
253 frequency bands, respectively. Rejected channels were interpolated using spherical splines
254 (Perrin, Pernier, Bertrand, & Echallier, 1989). Subsequently, noisy epochs were likewise
255 excluded based on FASTER and recursive outlier detection, resulting in the rejection of
256 approximately 13% of trials. To prevent trial rejection due to artifacts outside the signal of
257 interest, artifact detection was restricted to epochs that included 2.4 s of additional signal around
258 the on- and offset of the retention interval, corresponding to the longest effective segment that
259 was used in the analyses. A further 2.65% of incorrectly answered trials from the task were
260 subsequently excluded.

261
262 2.5 Rhythm-detection using extended BOSC

263
264 We applied an extended version of the Better OSCillation detection method (eBOSC;
265 cf. Caplan et al., 2001; Whitten et al., 2011) to automatically separate rhythmic from arrhythmic
266 episodes. The BOSC method reliably identifies rhythms using data-driven thresholds based on
267 theoretical assumptions of the signal characteristics. Briefly, the method defines rhythms as
268 time points during which wavelet-derived power at a particular frequency exceeds a *power*
269 *threshold* based on an estimate of the arrhythmic signal background. The theoretical *duration*
270 *threshold* defines a minimum duration of cycles this power threshold has to be exceeded to
271 exclude high amplitude transients. Previous applications of the BOSC method focused on the
272 analysis of resting-state data or long data epochs, where reliable detection has been established
273 regardless of specific parameter setups (Caplan et al., 2001; 2015; Whitten et al., 2011). We
274 introduce the following adaptations here (for details see section 2.6, Figures 1 & 2): (1) we
275 remove the spectral alpha peak and use robust regression to establish power thresholds; (2) we
276 combine detected time points into continuous rhythmic episodes and (3) we reduce the impact
277 of wavelet convolution on abundance estimates. We benchmarked the algorithm and compared
278 it to standard BOSC using simulations (see section 2.8).
279

RUNNING HEAD: SINGLE-TRIAL CHARACTERIZATION OF NEURAL RHYTHMS



280
 281 Figure 1: Schematic illustration of rhythm detection. (A) Average amplitude estimates (right)
 282 increase with the focus on rhythmic episodes within the averaged time interval. The left plots
 283 show simulated time series and the corresponding time-frequency power. Superimposed red
 284 traces indicate rhythmic time points. The upper right plot shows the average power spectrum
 285 averaged across the entire epoch, the lower plot presents amplitudes averaged exclusively
 286 across rhythmic time points. An amplitude gain is observed due to the exclusion of arrhythmic
 287 low amplitude time points. (B-E) Comparison of standard and extended BOSC. (B+C) Rhythms
 288 were detected based on a power threshold estimated from the arrhythmic background spectrum.
 289 Standard BOSC applies a linear fit in log-log space to define the background power, which may
 290 overestimate the background at the frequencies of interest in the case of data with large
 291 rhythmic peaks. Robust regression following peak removal alleviates this problem. (D)
 292 Example of episode detection. White borders circumscribe time frequency points, at which
 293 standard BOSC indicated rhythmic content. Red traces represent the continuous rhythmic
 294 episodes that result from the extended post-processing. (E) Applied thresholds and detected
 295 rhythmic abundance. The black border denotes the duration threshold at each frequency
 296 (corresponding to D), i.e., for how long the power threshold needed to be exceeded to count as
 297 a rhythmic period. Note that this threshold can be set to zero for a post-hoc characterization of
 298 the duration of episodes (see Methods 2.13). The color scaling within the demarcated area
 299 indicates the power threshold at each frequency. Abundance corresponds to the relative length
 300 of the segment on the same time scale as presented in D. White dots correspond to the standard
 301 BOSC measure of rhythmic abundance at each frequency (termed Pepisode). Red lines indicate

RUNNING HEAD: SINGLE-TRIAL CHARACTERIZATION OF NEURAL RHYTHMS

302 the abundance measure used here, which is defined as the proportion of sample points at which
303 a rhythmic episode between 8-15 Hz was indicated (shown as red traces in D).

304

305 2.6 Specifics of rhythm-detection using extended BOSC

306

307 Rhythmic events were detected within subjects for each channel and condition. Time-
308 frequency transformation of single trials was performed using 6-cycle Morlet wavelets
309 (Grossmann & Morlet, 1985) with 49 logarithmically-spaced center frequencies ranging from
310 1 to 64 Hz. Following the wavelet transform, 2 s were removed at each segment's borders to
311 exclude edge artefacts. To estimate the background spectrum, the time-frequency spectra from
312 all trials were temporally concatenated within condition and channel and log-transformed,
313 followed by temporal averaging. For eyes-closed and eyes-open resting states, both continuous
314 and interleaved exemplars were included in the background estimation for the respective
315 conditions. The resulting power spectrum was fit linearly in $\log(\text{frequency})\text{-}\log(\text{power})$
316 coordinates using a robust regression, with the underlying assumption that the EEG background
317 spectrum is characterized by colored noise of the form $A \cdot f^{-\alpha}$ (Buzsáki & Mizuseki, 2014;
318 He, Zempel, Snyder, & Raichle, 2010; Linkenkaer-Hansen, Nikouline, Palva, & Ilmoniemi,
319 2001). A robust regression with bisquare weighting (e.g. Holland & Welsch, 2007) was chosen
320 to improve the linear fit of the background spectrum (cf. Haller et al., 2018), which is
321 characterized by frequency peaks in the alpha range for almost all subjects (Supplementary
322 Figure 2). In contrast to ordinary least squares regression, robust regression iteratively down-
323 weights outliers (in this case spectral peaks) from the linear background fit. To improve the
324 definition of rhythmic power estimates as outliers during the robust regression, power estimates
325 within the wavelet pass-band around the individual alpha peak frequency were removed prior
326 to fitting¹. The passband of the wavelet (e.g. Linkenkaer-Hansen et al., 2001) was calculated as

¹ This procedure is similar to calculating the background spectrum from conditions with attenuated alpha power (e.g., the eyes open resting state; Caplan, Bottomley, Kang & Dixon (2015)). However, here we ensure that alpha power is sufficiently removed, whereas if conditions with reduced alpha peak magnitudes are selected, alpha power may still remain sufficiently elevated to influence slope or intercept estimates. Furthermore, the reliance on conditions with decreased rhythmicity appears less suitable given inter-individual differences in alpha engagement in e.g., the eyes open condition. This may induce an implicit contrast to

RUNNING HEAD: SINGLE-TRIAL CHARACTERIZATION OF NEURAL RHYTHMS

327
$$Passband [Hz] = IAF \pm 0.5 * \frac{2}{WL} * IAF$$

328 [Formula 1]

329 in which IAF denotes the individual alpha peak frequency and WL refers to wavelet length
330 (here, six cycles in the main analysis). IAF was determined based on the peak magnitude within
331 the 8-15 Hz average spectrum for each channel and condition (Grandy, Werkle-Bergner,
332 Chicherio, Schmiedek, et al., 2013b). This ensures that the maximum spectral deflection is
333 removed across subjects, even in cases where no or multiple peaks are present². This procedure
334 effectively removes a bias of the prevalent alpha peak on the arrhythmic background estimate
335 (see Figure 1B and C & Figure 4C). The power threshold for rhythmicity at each frequency was
336 set at the 95th percentile of a $\chi^2(2)$ -distribution of power values, centered on the linearly fitted
337 estimate of background power at the respective frequency (for details see Whitten et al., 2011).
338 This essentially implements a significance test of single-trial power against arrhythmic
339 background power. A three-cycle threshold was used as the duration threshold to exclude
340 transients, unless indicated otherwise (see section 2.13). The conjunctive power and duration
341 criteria produce a binary matrix of ‘detected’ rhythmicity for each time-frequency point (see
342 Figure 2C). To account for the duration criterion, 1000 ms were discarded from each edge of
343 this ‘detected’ matrix.

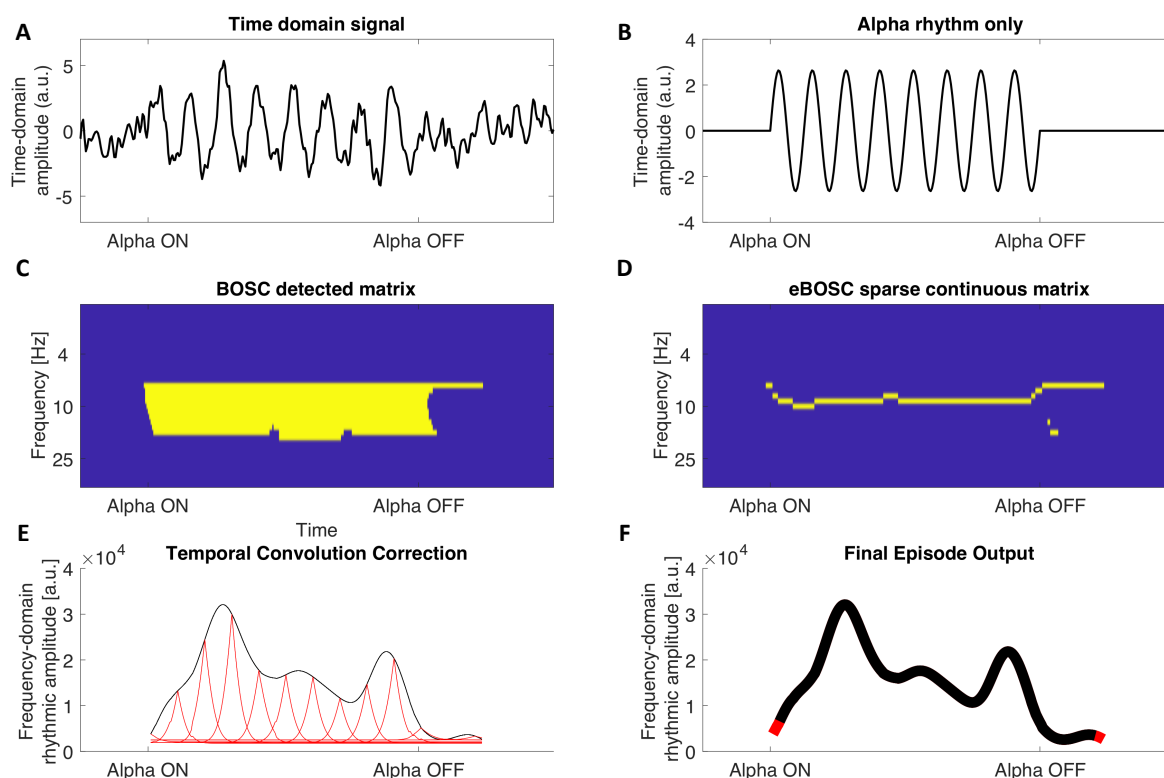
344

345

eyes open rhythmicity. Note that when the frequency range is chosen so that the alpha peak represents the middle of the chosen interval, the alpha-induced bias would be captured by a linear increment in the intercept of the background fit, which may also be alleviated by choosing a higher percentile for the power threshold. Notably, removing the alpha peak as done here attenuates such bias, even in cases where the alpha peak biases the slope of the background fit, as would happen if the alpha peak is not centered within the range of sampled frequencies.

² When multiple alpha-band peaks are present or the peak has a broader appearance, the spectral peak may not be removed entirely, which could result in misfits of the background spectrum. For this purpose, we employed robust regression to down-weight potential residuals around the alpha peak. Our current implementation only accounts for a peak in the alpha range, but could be extended to other frequency ranges using the same logic (see discussion on limitations in section 4.6).

RUNNING HEAD: SINGLE-TRIAL CHARACTERIZATION OF NEURAL RHYTHMS



346
347 Figure 2: Example of eBOSC's post-processing routines to derive sparse continuous rhythmic
348 'episodes'. (A) Simulated signal containing 1/f noise and superimposed 10 Hz rhythmicity. (B)
349 10 Hz rhythmic signal only. (C) Traditional output of BOSC detection: a binary matrix indicates
350 time-frequency points that adhere to power and duration thresholds (in yellow). These matrices
351 are used to calculate *Pepisode*. (D) First step of eBOSC's post-processing: the detected matrix
352 is 'sparsified' in the spectral dimension to create continuous rhythmic episodes. (E) Second
353 step of eBOSC's post-processing: each episode is temporally corrected for the temporal wavelet
354 convolution by estimating the bias of each time point on adjacent time points (here exemplified
355 for select time points via red traces). Only time points that exceed the bias estimated from
356 surrounding time points are retained. (F) Example of final episode trace. The black line
357 indicates the time points that were retained, whereas the red segments were removed during
358 step E. The final episode output is then characterized according to e.g., mean frequency,
359 duration and amplitude, whereas the time points of rhythmicity can for example be used to
360 define rhythm-conditional spectra. These episodes are used to calculate *abundance*.

361
362 The original BOSC algorithm was further extended to define rhythmic events as
363 continuous temporal episodes that allow for an event-wise assessment of rhythm characteristics
364 (e.g. duration). The following steps were applied to the binary matrix of 'detected' single-trial
365 rhythmicity to derive such sparse and continuous episodes. First, to account for the spectral
366 extension of the wavelet, we selected time-frequency points with maximal power within the

RUNNING HEAD: SINGLE-TRIAL CHARACTERIZATION OF NEURAL RHYTHMS

367 wavelet's spectral smoothing range (i.e. the pass-band of the wavelet; $\frac{2}{WL}$ *frequency; see
368 Formula 1). That is, at each time point, we selected the frequency with the highest indicated
369 rhythmicity within each frequency's pass-band. This served to exclude super-threshold
370 timepoints that may be accounted for by spectral smoothing of a rhythm at an adjacent
371 frequency. Note that this effectively creates a new frequency resolution for the resulting
372 rhythmic episodes, thus requiring sufficient spectral resolution (defined by the wavelet's pass-
373 band) to differentiate simultaneous rhythms occurring at close frequencies. Finally, continuous
374 rhythmic episodes were formed by temporally connecting extracted time points, while allowing
375 for moment-to-moment frequency transitions (i.e. within-episode frequency non-stationarities;
376 Atallah & Scanziani, 2009) (for a single-trial illustration see Figures 1D and 2D).

377 In addition to the spectral extension of the wavelet, the choice of wavelet parameter also
378 affects the extent of temporal smoothing, which may bias rhythmic duration estimates. To
379 decrease such temporal bias, we compared observed rhythmic amplitudes at each time point
380 within each rhythmic episode with those expected by smoothing adjacent amplitudes using the
381 wavelet (Figure 2E). By retaining only those time points where amplitudes exceeded the
382 smoothing-based expectations, we removed supra-threshold time points that can be explained
383 by temporal smoothing of nearby rhythms (e.g., 'ramping' up and down signals). In more detail,
384 we simulated the positive cycle of a sine wave at each frequency, zero-shouldered each edge
385 and performed (6-cycle) wavelet convolution. The resulting amplitude estimates at the zero-
386 padded time points reflect the temporal smoothing bias of the wavelet on adjacent arrhythmic
387 time points. This bias is maximal (*BiasMax*) at the time point immediately adjacent to the
388 rhythmic on-/offset and decreases with temporal distance to the rhythm. Within each rhythmic
389 episode, the 'convolution bias' of a time-frequency (TF) point's amplitude on surrounding
390 points was estimated by scaling the points' amplitude by the modelled temporal smoothing bias.

$$391 \quad Amplitudes_{F,T+1-L:L-T} = \left[(Amplitude_{TF} - PT_F) * \frac{BiasVector_{F,T+1-L:L-T}}{BiasMax_F} \right] + PT_F$$

392 [Formula 2]

393 Subscripts F and T denote frequency and time within each episode, respectively.
394 *BiasVector* is a vector with the length of the current episode (L) that is centered around the
395 current TF-point. It contains the wavelet's symmetric convolution bias around *BiasMax*. Note
396 that both *BiasVector* and *BiasMax* respect the possible frequency variations within an episode
397 (i.e., they reflect the differences in convolution bias between frequencies). The estimated
398 wavelet bias was then scaled to the amplitude of the rhythmic signal at the current TF-point.
399 PT refers to the condition- and frequency-specific power threshold applied during rhythm

RUNNING HEAD: SINGLE-TRIAL CHARACTERIZATION OF NEURAL RHYTHMS

400 detection. We subtracted the power threshold to remove arrhythmic contributions. This
401 effectively sensitizes the algorithm to near-threshold values, rendering them more likely to be
402 excluded. Finally, time points with lower amplitudes than expected by the convolution model
403 were removed and new rhythmic episodes were created (Figure 2F). The resulting episodes
404 were again checked for adhering to the duration threshold.

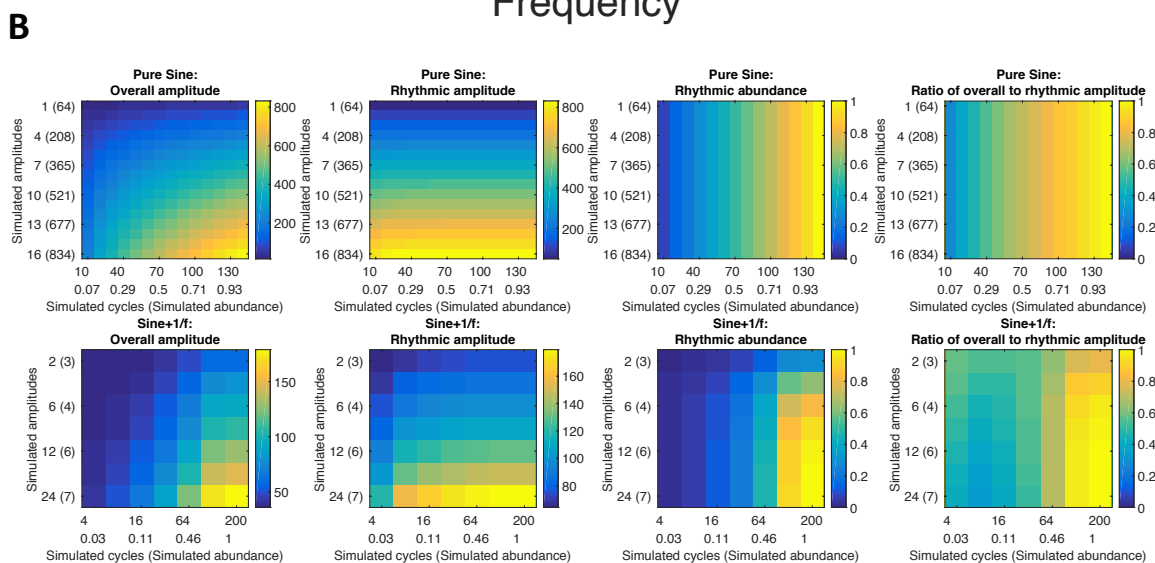
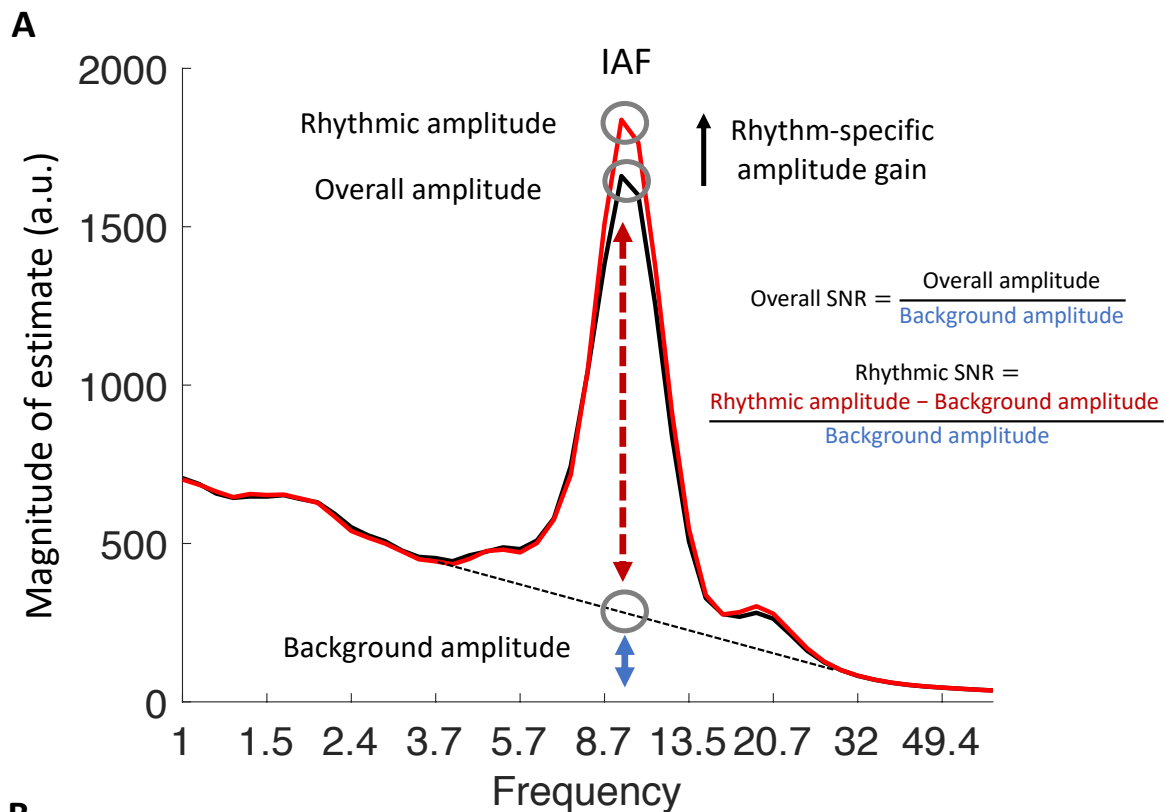
405 As an alternative to the temporal wavelet correction based on the wavelet's simulated
406 maximum bias ('MaxBias'; as described above), we investigated the feasibility of using the
407 wavelet's full-width half maximum ('FWHM') as a criterion. Within each continuous episode
408 and for each "rhythmic" sample point, 6-cycle wavelets at the frequency of the neighbouring
409 points were created and scaled to the point's amplitude. We then used the amplitude of these
410 wavelets at the FWHM as a threshold for rhythmic amplitudes. That is, points within a rhythmic
411 episodes that had amplitudes below those of the scaled wavelets were defined as arrhythmic.
412 The resulting continuous episodes were again required to pass the duration threshold. As the
413 FWHM approach indicated decreased specificity of rhythm detection in the simulations
414 (Supplementary Figure 1) we used the 'MaxBias' method for our analyses.

415 Furthermore, we considered a variant where total amplitude values were used (vs.
416 supra-threshold amplitudes) as the basis for the temporal wavelet correction. Our results
417 suggest that using supra-threshold power values leads to a more specific detection at the cost
418 of sensitivity (Supplementary Figure 1). Crucially, this eliminated false alarms and abundance
419 overestimation, thus rendering the method highly specific to the occurrence of rhythmicity. As
420 we regard this as a beneficial feature, we used supra-threshold amplitudes as the basis for the
421 temporal wavelet correction throughout the manuscript.

422

423 2.7 Definition of abundance, rhythmic probability and amplitude metrics

424



425
426
427
428
429
430
431
432
433
434

Figure 3: eBOSC disambiguates the magnitude and duration of rhythmic episodes. (A) Schema of different amplitude metrics. (B) Rhythm-detection disambiguates rhythmic amplitude and duration. Overall amplitudes represent a mixture of rhythmic power and duration. In the absence of noise (upper row), eBOSC perfectly orthogonalizes rhythmic amplitude from abundance. Superimposed noise leads to an imperfect separation of the two metrics (lower row). The duration of rhythmicity is similarly indicated by abundance and the overlap between rhythmic and overall amplitudes. This can be seen by comparing the two rightmost plots in each row.

435

436 A central goal of rhythm detection is to disambiguate rhythmic power and duration
 437 (Figure 3). For this purpose, eBOSC provides multiple indices. We describe the different
 438 indices for the example case of alpha rhythms. Please note that eBOSC can be applied in a
 439 similar fashion to any other frequency range. The **abundance** of alpha rhythms denotes the
 440 duration of rhythmic episodes with a mean frequency in the alpha range (8 to 15 Hz), relative
 441 to the duration of the analyzed segment. This frequency range was motivated by clear peaks
 442 within this range in individual resting state spectra (Supplementary Figure 2). Note that
 443 abundance is closely related to standard BOSC’s Pepisode metric (Whitten et al., 2011), with
 444 the difference that abundance refers to the duration of the continuous rhythmic episodes and
 445 not the ‘raw’ detected rhythmicity of BOSC (cf. Figure 2C and D). We further define **rhythmic**
 446 **probability** as the *across trials* probability to observe a detected rhythmic episode within the
 447 alpha frequency range at a given point in time. It is therefore the within-time, across-trial
 448 equivalent of abundance.

449 As a result of rhythm detection, the magnitude of spectral events can be described using
 450 multiple metrics (see Figure 3A for a schematic). The standard measure of window-averaged
 451 amplitudes, **overall amplitudes** were computed by averaging across the entire segment at its
 452 alpha peak frequency. In contrast, **rhythmic amplitudes** correspond to the amplitude estimates
 453 during detected rhythmic episodes. If no alpha episode was indicated, abundance was set to
 454 zero, and amplitude was set to missing. Unless indicated otherwise, both amplitude measures
 455 were normalized by subtracting the amplitude estimate of the fitted background spectrum. This
 456 step represents a parameterization of rhythmic power (cf. Haller et al., 2018) and is conceptually
 457 similar to baseline normalization, without requiring an explicit baseline segment. This
 458 highlights a further advantage of rhythm-detection procedures like (e)BOSC. In addition, we
 459 calculated an **overall signal-to-noise ratio (SNR)** as the ratio of the overall amplitude to the
 460 background amplitude: $\frac{Overall}{Background}$. In addition, we defined **rhythmic SNR** as the background-
 461 normalized rhythmic amplitude as a proxy for the rhythmic representation:
 462 $\frac{Rhythmic-Background}{Background}$. Unless stated differently, subject-, and condition-specific amplitude and
 463 abundance values were averaged within and across trials, and across posterior-occipital
 464 channels (P7, P5, P3, P1, Pz, P2, P4, P6, P8, PO7, PO3, POz, PO4, PO8, O1, Oz, O2), in which
 465 alpha power was maximal (Figure 5A, Figure 11).

466

467 2.8 eBOSC validation via alpha rhythm simulations

468

469 To assess eBOSC's detection performance, we simulated 10 Hz sine waves with varying
470 amplitudes (0, 2, 4, 6, 8, 12, 16, 24 [a.u.]) and durations (2, 4, 8, 16, 32, 64, 128, 200 [cycles])
471 that were symmetrically centred within random 1/f-filtered white noise signals (20 s; 250 Hz
472 sampling rate). Amplitudes were scaled relative to the power of the 8-12 Hz 6th order
473 Butterworth-filtered background signal in each trial to approximate SNRs. To ensure
474 comparability with the empirical analyses, we computed overall SNR analogously to the
475 empirical data, which tended to be lower than the target SNR. We chose the maximum across
476 simulated durations as an upper bound (i.e., conservative estimate) on overall SNR. For each
477 amplitude-duration combination we simulated 500 "trials". We assessed three different
478 detection pipelines regarding their detection efficacy: the standard BOSC algorithm (i.e., linear
479 background fit incorporating the entire frequency range with no post-editing of the detected
480 matrix); the eBOSC method using wavelet correction by simulating the maximum bias
481 introduced by the wavelet ("MaxBias"); and the eBOSC method using the full-width-at-half-
482 maximum amplitude for convolution correction ("FWHM"). The background was estimated
483 separately for each amplitude-duration combination. 500 edge points were removed bilaterally
484 following wavelet estimation, 250 additional samples were removed bilaterally following
485 BOSC detection to account for the duration threshold, effectively retaining 14 s of simulated
486 signal.

487 Detection efficacy was indexed by signal detection criteria regarding the identification
488 of rhythmic time points between 8 and 12 Hz (i.e., hits = simulated and detected points; false
489 alarms = detected, but not simulated points). These measures are presented as ratios to the full
490 amount of possible points within each category (e.g., hit rate = hits/all simulated time points).
491 For the eBOSC pipelines, abundance was calculated identically to the analyses of empirical
492 data. As no consecutive episodes (cf. Pepisode and abundance) are available in standard BOSC,
493 abundance was defined as the relative amount of time points with detected rhythmicity between
494 8 to 12 Hz.

495 A separate simulation aimed at establishing the ability to accurately recover amplitudes.
496 For this purpose, we simulated a whole-trial alpha signal (i.e., duration = 1) and a quarter-trial
497 alpha signal (duration = .25) with a larger range of amplitudes (1:16 [a.u.]) and performed
498 otherwise identical procedures as described above. To assess eBOSC's ability to disambiguate
499 power and duration (Figure 3B), we additionally performed simulations in the absence of noise
500 across a larger range of simulated amplitudes and durations.

501 A major change in eBOSC compared to standard BOSC is the exclusion of the rhythmic
 502 peak prior to estimating the background. To investigate to what extent the two methods induce
 503 a bias between rhythmicity and the estimated background magnitude (for a schematic see Figure
 504 1C and D), we calculated Pearson correlations between the overall amplitude and the estimated
 505 background amplitude across all levels of simulated amplitudes and durations (Figure 4C).

506 As the empirical data suggested a trial-wise association between amplitude and
 507 abundance estimates also at high levels of signal-to-noise ratios (Figure 8), we investigated
 508 whether such associations were also present in the simulations. For each pair of simulated
 509 amplitude and duration, we calculated Pearson correlations between the overall amplitude and
 510 abundance across single trials. Note that due to the stationarity of simulated duration, trial-by-
 511 trial fluctuations indicate the bias under fluctuations of the noise background (as amplitudes
 512 were scaled to the background in each trial). For each cell, we performed Fisher's r-to-z
 513 transform to account for unequal trial sizes due to missing amplitude/abundance estimates (e.g.
 514 when no episodes are detected).

515

516 2.9 Calculation of phase-based lagged coherence

517

518 To investigate the convergence between the power-based duration estimate (abundance)
 519 and a phase-based alternative, we calculated lagged coherence at 40 linearly scaled frequencies
 520 in the range of 1 to 40 Hz for each resting-state condition. Lagged coherence assesses the
 521 consistency of phase clustering at a single sensor for a chosen cycle lag (see Fransen et al., 2015
 522 for formulas). Instantaneous power and phase were estimated via 3-cycle wavelets. Data were
 523 segmented to be identical to eBOSC's effective interval (i.e., same removal of signal shoulders
 524 as described above). In reference to the duration threshold for power-based rhythmicity, we
 525 calculated the averaged lagged coherence using two adjacent epochs à three cycles. We
 526 computed an index of alpha rhythmicity by averaging values across epochs and posterior-
 527 occipital channels, finally extracting the value at the maximum lagged coherence peak in the 8
 528 to 15 Hz range.

529

530 2.10 Dynamics of rhythmic probability and rhythmic power during task performance

531

532 To investigate the detection properties in the task data, we analysed the temporal
 533 dynamics of rhythmic probability and power in the alpha band. We created time-frequency
 534 representations as described in section 2.6 and extracted the IAF power time series, separately

535 for each person, condition, channel and trial. At the single-trial level, values were allocated to
 536 rhythmic vs. arrhythmic time points according to whether a rhythmic episode with mean
 537 frequency in the respective range was indicated by eBOSC (Figure 2B; Figure 3C). These time
 538 series were averaged within subject to create individual averages of rhythm dynamics.
 539 Subsequently, we z-scored the power time series to accentuate signal dynamics and attenuate
 540 between-subject power differences. To highlight global dynamics, these time series were
 541 further averaged within- and between-subjects. Figure captions indicate which average was
 542 used.

543

544 2.11 Rhythmic frequency variability during rest

545

546 As an exemplary characteristic of rhythmicity, we assessed the stability of IAF
 547 estimates by considering the variability across trials of the task as a function of indicated
 548 rhythmicity. Trial-wise rhythmic IAF variability (Figure 10A) was calculated as the standard
 549 deviation of the mean frequency of alpha episodes (8-15 Hz). That is, for each trial, we averaged
 550 the estimated mean frequency of rhythmic episodes within that trial and computed the standard
 551 deviation across trials. Whole-trial IAF variability (Figure 10B) was similarly calculated as the
 552 standard deviation of the IAF, with single-trial IAF defined as the frequency with the largest
 553 peak magnitude between 8-15 Hz, averaged across the whole trial, i.e., encompassing segments
 554 both designated as rhythmic and arrhythmic. Finally, we compared the empirical variability
 555 with that observed in simulations (see section 2.8).

556

557 2.12 Rhythm-conditional spectra and abundance for multiple canonical frequencies

558

559 To assess the general feasibility of rhythm detection outside the alpha range, we analysed the
 560 retention interval of the adapted Sternberg task, where the occurrence of theta, alpha and beta
 561 rhythms has been reported in previous studies (Brookes et al., 2011; Jensen, Gelfand, Kounios,
 562 & Lisman, 2002; Jokisch & Jensen, 2007; Lundqvist et al., 2016; Raghavachari et al., 2001;
 563 Tuladhar et al., 2007). For this purpose, we re-segmented the data to cover the final 2 s of the
 564 retention interval +/- 3 s of edge signal that was removed during the eBOSC procedure. We
 565 performed eBOSC rhythm detection with otherwise identical parameters to those described in
 566 section 2.6. We then calculated spectra across those time points where rhythmic episodes with
 567 a mean frequency in the range of interest were indicated, separately for four frequency ranges:
 568 3-8 Hz (theta), 8-15 Hz (alpha), 15-25 Hz (beta) and 25-64 Hz (gamma). We subtracted spectra

569 across the remaining arrhythmic time-points for each range from these ‘rhythm-conditional’
 570 spectra to derive the spectra that are unique to those time points with rhythmic occurrence in
 571 the band of interest.

572 For the corresponding topographic representations, we calculated the abundance metric
 573 as described in section 2.7 for the apparent peak frequency ranges.

574

575 2.13 Post-hoc characterization of sustained rhythms vs. transients

576

577 Instead of exclusively relying on a fixed *a priori* duration threshold as done in previous
 578 applications, eBOSC’s continuous ‘rhythmic episodes’ also allow for a post-hoc separation of
 579 rhythms and transients based on the duration of identified rhythmic episodes. This is afforded
 580 by our extended post-processing that results in a more specific identification of rhythmic
 581 episodes (see Figure 4) and an estimated length for each episode. For this analysis (Figure 14),
 582 we set the *a priori* duration threshold to zero and separated the resulting episodes post-hoc
 583 based on their duration (shorter vs. longer than 3 cycles) at their mean frequency. That is, any
 584 episode crossing the amplitude threshold was retained and episodes were sorted by their
 585 ‘transient’ or sustained appearance afterwards. We conducted this analysis in the extended task
 586 data to highlight the temporal dynamics of rhythmic and transient events.

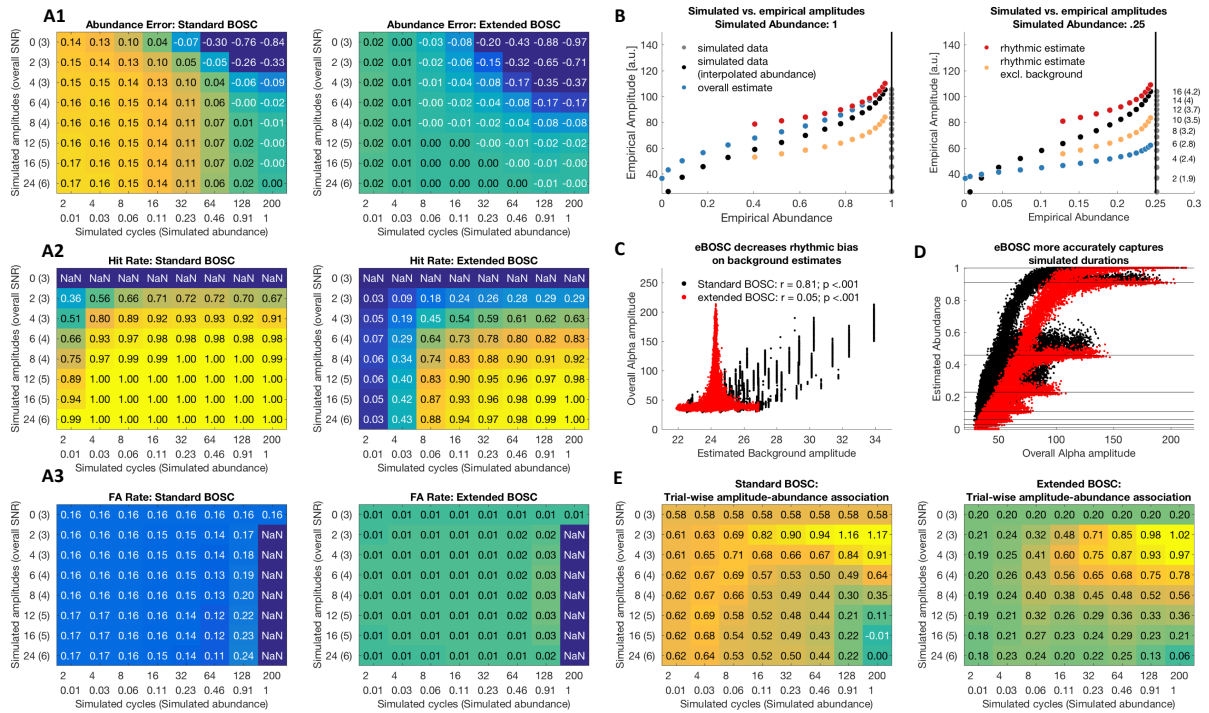
587 Similarly, the temporal specificity of rhythmic episodes allow the assessment of
 588 ‘rhythm-evoked’ effects in the temporal or spectral domain. Here, we showcase the rhythm-
 589 evoked changes in the same frequency band to indicate the temporal specificity of the indicated
 590 rhythmic periods (Figure 15). For this purpose, we calculated time-frequency representations
 591 using 6-cycle wavelets and extracted power in the theta (3-8 Hz), alpha (8-15 Hz), beta (15-25
 592 Hz) and gamma-band (25-64 Hz) in 2.4 s periods centred on the on- and offset of indicated
 593 rhythmic periods in the respective band. Separate TFRs were calculated for the detected
 594 episodes in each channel, followed by averaging across episodes and channels. Finally, we z-
 595 transformed the individual averages to highlight the consistency across subjects.

596

597 **3. Results**

598

599 3.1. Extended BOSC (eBOSC) increases specificity of rhythm-detection



600
 601 Figure 4: Rhythm detection performance of standard and extended BOSC in simulations. (A)
 602 Signal detection properties of the two algorithms. For short simulated rhythmicity, abundance
 603 is overestimated by standard BOSC, but not eBOSC, whereas eBOSC underestimates the
 604 duration of prolonged rhythmicity at low SNRs (A1). Extended BOSC has decreased sensitivity
 605 (A2), but higher specificity (A3) compared with extended BOSC. Note that for simulated zero
 606 alpha amplitude, all sample points constitute potential false alarms, while by definition no
 607 sample point constitutes a potential hit. (B) Amplitude and abundance estimates for signals with
 608 sustained (left) and short rhythmicity (right). Black dots indicate reference estimates for a pure
 609 sine wave without noise, coloured dots indicate the respective estimates for data with the 1/f
 610 background. [Note that the reference estimates were interpolated at the empirical abundance of
 611 the 1/f data. Grey dots indicate the perfect abundance estimates in the absence of background
 612 noise.] When rhythms are sustained (left), impaired rhythm detection at low SNRs causes an
 613 overestimation of the rhythmic amplitude. At low rhythmic duration (right), this deficit is
 614 outweighed by the severe bias of arrhythmic duration on overall amplitude estimates (e.g.,
 615 Figure 13). Simulated amplitudes (and corresponding empirical SNRs in brackets) are shown
 616 on the right. Vertical lines indicate the simulated rhythmic duration. (C) eBOSC successfully
 617 reduces the bias of the rhythmic peak on the estimation of the background amplitude. In
 618 comparison, standard BOSC induces a strong coupling between the peak magnitude and the
 619 background estimate. (D) eBOSC indicates abundance more accurately than standard BOSC at

620 high amplitudes (i.e., high SNR; see also A1). The leftward shift indicates a decrease in
 621 sensitivity. Horizontal lines indicate different levels of simulated duration. Dots are single-trial
 622 estimates across levels of simulated amplitude and duration. (E) Standard BOSC and eBOSC
 623 induce trial-wise correlations between amplitude and abundance. eBOSC exhibits reduced trial-
 624 by-trial coupling at higher SNR compared to standard BOSC. Values are r-to-z-transformed
 625 correlation coefficients.

626

627 We extended the BOSC rhythm detection method to characterize rhythmicity at the
 628 single-trial level by creating continuous ‘rhythmic episodes’ (see Figure 1 & 2). A central goal
 629 of this approach is the disambiguation of rhythmic power and duration (see Figure 3). In
 630 situations without background noise, this can be achieved perfectly. However, the addition of
 631 1/f noise leads to a partial coupling of the two parameters. As we introduced changes to the
 632 original method, we compared the detection properties of the standard and the extended
 633 (eBOSC) pipeline by simulating varying levels of rhythm magnitude and duration.

634 Considering the sensitivity and specificity of detection, both pipelines performed
 635 adequately at high levels of SNR with high hit and low false alarm rates (Figure 4A). However,
 636 we observed important differences between the algorithms. While standard BOSC showed
 637 perfect sensitivity above overall SNRs of ~ 4 , specificity was lower than for eBOSC as indicated
 638 by higher false alarm rates (grand averages: .160 for standard BOSC; .015 for eBOSC). This
 639 specificity increase is observed across simulation parameters, suggesting a general abundance
 640 overestimation by standard BOSC (see also Figure 4D). In addition, standard BOSC did not
 641 show a reduced detection of transient rhythms below the duration threshold of three cycles,
 642 whereas hit rates for those transients were clearly reduced in eBOSC (Figure 4A2). This
 643 suggests that wavelet-convolution extended the effective duration of transient rhythmic
 644 episodes, resulting in an exceedance of the temporal threshold. In contrast, by creating explicit
 645 rhythmic episodes and reducing convolution effects, eBOSC more strictly adheres to the
 646 specified target duration. However, there was also a notable reduction in sensitivity for rhythms
 647 just above the duration threshold, suggesting a sensitivity-specificity trade-off (Figure 4A2).
 648 In addition to decreasing false alarms, eBOSC also more accurately estimated the duration of
 649 rhythmicity (Figure 4A1), although an underestimation of abundance persisted (and was
 650 increased) at low SNRs. In sum, while eBOSC improves the specificity of identifying rhythmic
 651 content, there are also noticeable decrements in sensitivity (grand averages: .909 for standard
 652 BOSC; .614 for eBOSC), especially at low SNRs. Notably, while sensitivity remains an issue,

653 the high specificity of detection suggests that the estimated rhythmic abundance serves as a
654 lower bound on the actual duration of rhythmicity.

655 In a second set of simulations, we considered eBOSC's potential to accurately estimate
656 rhythmic amplitudes. As expected, in signals with stationary rhythms (duration = 1), the overall
657 amplitude most accurately represented the simulated amplitude (Figure 4B left), as any
658 methods-induced underestimation would introduce inaccuracies. Hence, at lower SNRs,
659 underestimation of rhythmic content resulted in an overestimation of rhythmic power, as some
660 low-amplitude time points were incorrectly excluded prior to averaging. At those low SNRs,
661 subtraction of the background estimate (cf. baseline normalization) alleviates this
662 overestimation. The general impairment at low SNRs is however outweighed by the advantage
663 of rhythm-specific amplitude estimates in time series where rhythmic duration is low and thus
664 arrhythmicity is prevalent (Figure 4B right). Here, rhythm-specific estimates accurately track
665 simulated amplitudes, whereas a strong underestimation is observed for unspecific power
666 indices. We again observed an underestimation of rhythmic duration with decreasing
667 amplitudes (as in Figure 4A1).

668 An adaptation of the eBOSC method is the exclusion of the rhythmic alpha peak prior
669 to fitting the arrhythmic background. This serves to reduce a potential bias of rhythmic content
670 on the estimation of the arrhythmic content (see Figure 1C for a schematic). Our simulations
671 indeed indicate a bias of the spectral peak amplitude on the background estimate in the standard
672 BOSC algorithm, which is substantially reduced in eBOSC (Figure 4C).

673 To gain a visual representation of duration estimation performance, we plotted
674 abundance against amplitude estimates across all simulated trials, regardless of simulation
675 parameters (Figure 4D). This reveals multiple modes of abundance at high levels of amplitude,
676 which in the eBOSC case more closely track the simulated duration. This further visualizes the
677 decreased error in abundance estimates, especially at high SNRs (e.g., Figure 4A), while an
678 observed rightward shift towards higher amplitudes indicated the more pronounced
679 underestimation of rhythmicity when SNRs are low.

680 Finally, we investigated the trial-wise association between amplitude and duration
681 estimate based on the observed coupling in empirical data (see Figure 8). Our simulations
682 suggest that both standard BOSC and eBOSC can induce spurious positive correlations between
683 amplitude and abundance estimates, which are most pronounced at low levels of SNR (Figure
684 4E). Notably, these associations are strongly reduced in eBOSC, especially when rhythmic
685 power is high. While this suggests a remaining methods-induced association between the two

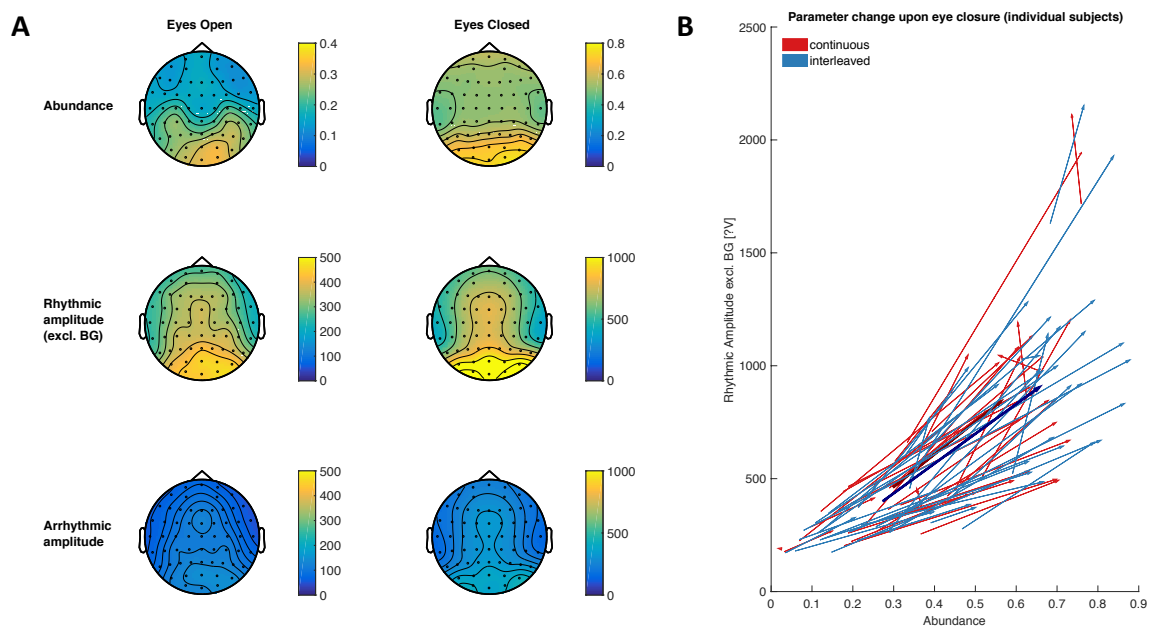
686 parameters, it also indicates that eBOSC provides a better separation between the two (here
687 independently simulated) parameters.

688 In sum, our simulations suggest that eBOSC specifically separates rhythmic and
689 arrhythmic time points in simulated data at the expense of decreased sensitivity, especially
690 when SNR is low. However, the increase in specificity is accompanied by an increased accuracy
691 of duration estimates at high SNR, theoretically allowing a more precise investigation of
692 rhythmic duration.

693

694 3.2 eBOSC detects single-trial alpha rhythms during rest and task states

695



696
697 Figure 5: Rhythmic abundance and amplitude during rest. (A) eBOSC identifies high occipital
698 alpha abundance and rhythmic amplitude especially during the Eyes Closed resting state. (B)
699 Eye closure modulates both rhythmic amplitude and abundance on an individual level. Arrows
700 indicate the direction and magnitude of parameter change upon eye closure for each subject.
701 Red arrows indicate data during continuous eyes closed/eyes open intervals, blue arrows
702 represent data from the interleaved acquisition. Thick arrows indicate the group average.

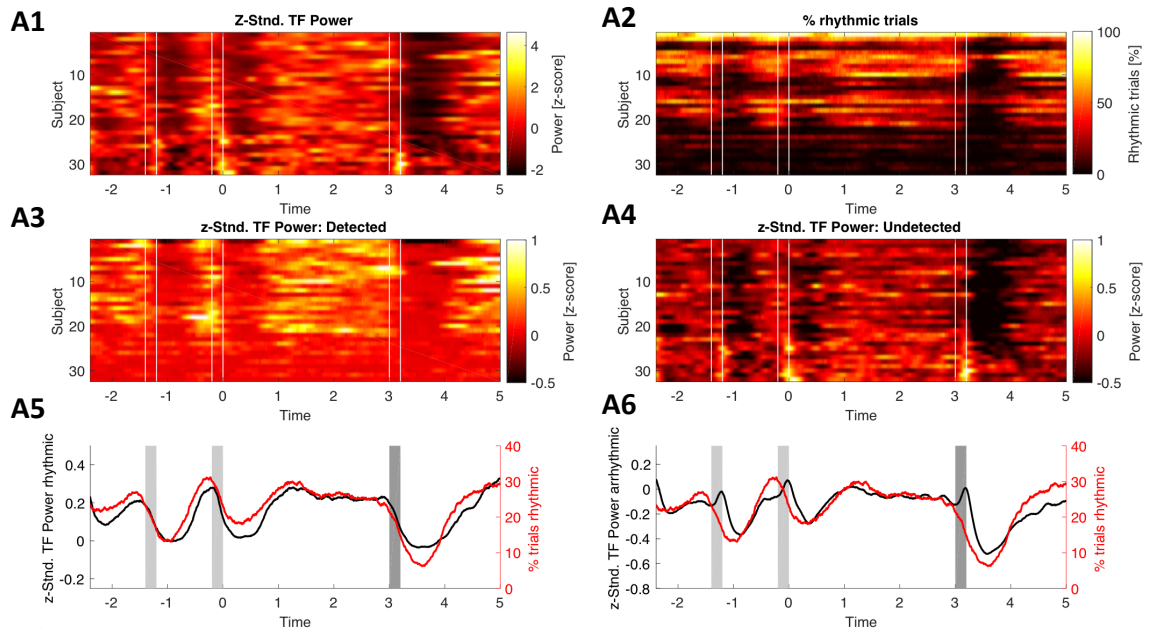
703

704 While the simulations provide a gold standard to assess detection performance, we
705 further probed eBOSC's detection performance in empirical data from resting and task states
706 to investigate the practical feasibility and utility of rhythm detection. As the ground truth in real

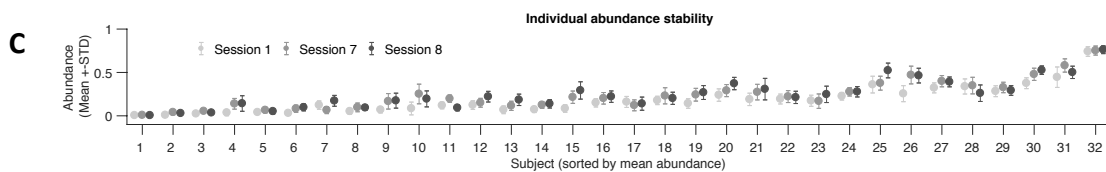
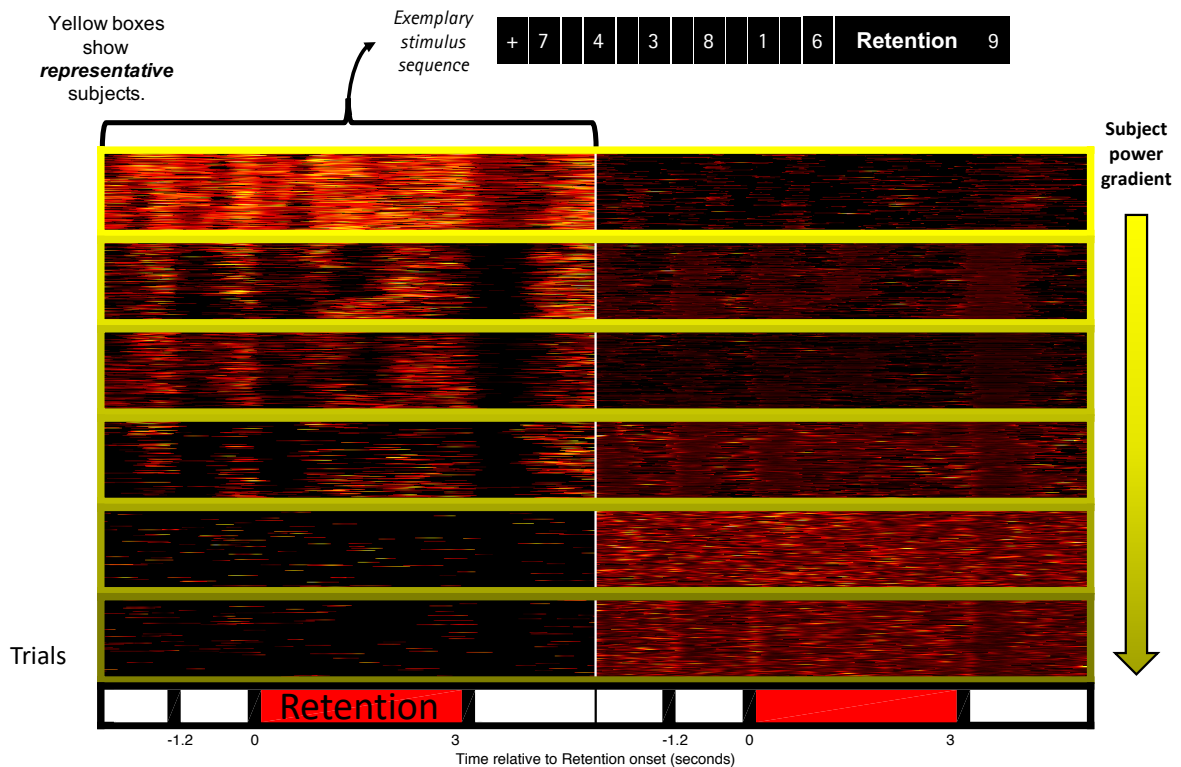
707 data is unknown, we evaluated detection performance by contrasting metrics from detected and
708 undetected timepoints regarding their topography and time course.

709 Individual power spectra showed clear rhythmic alpha peaks for every participant
710 during eyes closed rest and for most subjects during eyes open rest and the task retention period,
711 indicating the general presence of alpha rhythms during the analysed states (Supplementary
712 Figure 2). In line with a putative source in visual cortex, alpha abundance was highest over
713 parieto-occipital channels during the resting state (Figure 5A) and during the WM retention
714 period (Figure 11). As expected, rhythmic time-points exhibited increased alpha power
715 compared with arrhythmic time points (Figure 5A). In addition, alpha power and abundance
716 underwent state modulations. As one of the earliest findings in cognitive electrophysiology
717 (Berger, 1938), alpha amplitudes increase in magnitude upon eye closure. Here, eye closure
718 was reflected by a joint shift towards higher amplitudes and durations for almost all participants
719 (Figure 5B), suggesting that both parameters similarly reflected the state shift.

RUNNING HEAD: SINGLE-TRIAL CHARACTERIZATION OF NEURAL RHYTHMS



B Detected/non-detected masked power values @ IAF (8-15 Hz) @ O2



720

721 Figure 6: Characterization of detected single-trial rhythmicity during task performance. (A)

722 Average evoked alpha power and rhythmic probability at posterior-occipital channels. (A1-A4)

723 Individual dynamics of power and rhythmicity. (A5) Rhythmic power at IAF (blue) and rhythm
 724 probability (red) exhibit stereotypic temporal dynamics during encoding (red bars), retention
 725 (0 to 3 s) and retrieval (black bars). (A6) While arrhythmic power exhibits similar temporal
 726 dynamics, it is strongly reduced in power (see scales in A5 and A6). The arrhythmic power
 727 dynamics are characterized by additional transient increases following stimulus presentations
 728 (blue vs. red traces between vertical bars; cf., A6). Data are from the first session and the high
 729 load condition. (B) Task-related alpha dynamics are captured by eBOSC at the single-trial level.
 730 Each box displays individual trial-wise z-standardized IAF alpha power, separately for
 731 rhythmic (left) and non-rhythmic (right) time points. While rhythmic time points (left) exhibit
 732 clear single-trial power increases that are locked to the task design, arrhythmic time points
 733 (right) do not show evoked task dynamics that separate them from the background, hence
 734 suggesting an accurate rejection of rhythmicity. The subplots' frame colour indicates the
 735 subjects' raw power maximum (i.e., the data scaling). Data are from channel O2 during the first
 736 session across load conditions. (C) Individual abundance estimates are stable across sessions.
 737 Data were averaged across posterior-occipital channels and high (i.e., 6) item load trials.

738

739 The temporal dynamics of indicated rhythmicity are another characteristic of interest,
 740 which we assessed by considering the rhythmic probability across trials at each time point.
 741 While such an investigation is difficult for induced rhythmicity during rest, evoked rhythmicity
 742 offers an optimal test case due to its systematic temporal deployment. For this reason, we
 743 analysed task recordings with stereotypic design-locked alpha power dynamics at encoding,
 744 retention and probe presentation (Figure 6AB). At the average level, rhythmic probability
 745 closely tracked power dynamics (Figure 6A) and time points designated as rhythmic exhibited
 746 pronounced alpha power compared with those labelled arrhythmic (6A3 vs. 6A4; 6A5 vs. 6A6).
 747 While rhythm-specific dynamics were closely capturing standard power trajectories, we
 748 observed a dissociation concerning arrhythmic power. Here, we observed transient increases
 749 during stimulus onsets that were absent from either abundance or rhythmic power (Figure 6A6).
 750 This suggests an increase in high-power transients that were excluded due to the 3 cycle
 751 duration threshold. Indeed, an increase in transient events was observed without an *a priori*
 752 duration threshold (see Figure 14). In sum, these results suggest an accurate detection at the
 753 average level. However, we also observed large inter-individual variability in detected
 754 rhythmicity (Figure 6A2). Such result is consistent with the prevalence of shorter rhythmicity
 755 or a general absence of rhythmic content. To resolve this ambiguity, we investigated detection
 756 in single trials.

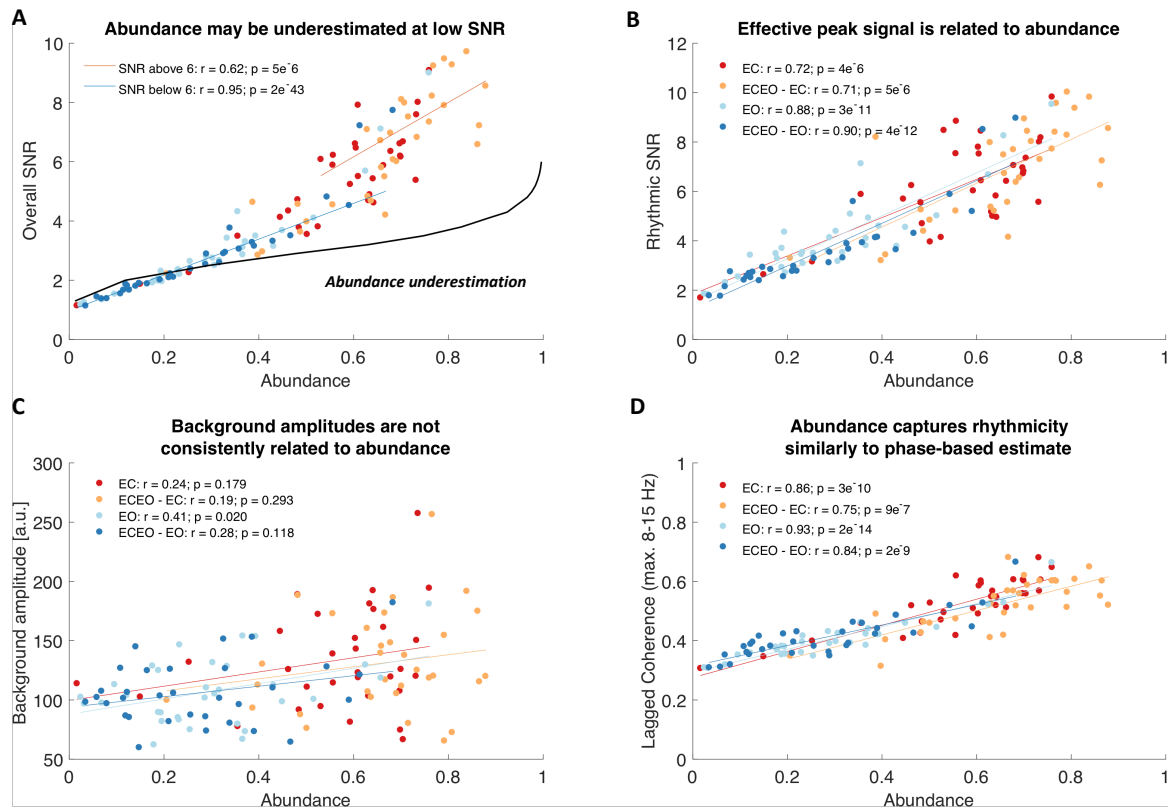
757 At the single-trial level, rhythmicity was indicated for periods with visibly elevated
758 alpha power with strong task-locking (Figure 6B left). Conversely, arrhythmicity was indicated
759 for time points with low alpha power and little structured dynamics (Figure 6B right). However,
760 strong inter-individual differences were apparent, with little detected rhythmicity when global
761 alpha power was low (Figure 6B bottom; plots are sorted by descending power as indicated by
762 the frame colour of the depicted subjects and scaled using z-scores to account for global power
763 differences). Crucially, those subjects' single-trial power dynamics did not present a clear
764 temporal structure, suggesting a prevalence of noise and therefore a correct rejection of
765 rhythmicity.

766 Notably, individual rhythmicity estimates were stable across multiple sessions (Figure
767 6C), suggesting that they are indicative of trait-like characteristics rather than idiosyncratic
768 measurement noise (Grandy et al., 2013). Note that it is unlikely that such detection differences
769 are primarily due to misfits of the background spectrum. Simulations suggest that compared to
770 the linear background fit that is implemented in standard BOSC, the robust fit with alpha peak
771 removal successfully removes the bias of rhythmic alpha power on background estimates
772 (Figure 4C), while individual power thresholds indicate a successful exclusion of the alpha peak
773 (Supplementary Figure 2).

774 In sum, these results suggest that eBOSC successfully separates rhythmic and
775 arrhythmic episodes in empirical data, both at the group and individual level. However, they
776 also suggest prevalent and stable differences in single-trial rhythmicity in the alpha band.

777

778 3.3 Rhythmic SNR constrains indicated rhythmicity and rhythm-related metrics



779

780 Figure 7: Inter-individual alpha abundance is strongly associated with rhythmic, but not
 781 arrhythmic power and may be underestimated at low rhythmic SNR. **(A)** Individual abundance
 782 estimates are strongly related to the overall SNR of the spectral alpha peak. This relationship is
 783 also observed when only considering individual data within the SNR range for which simulation
 784 analyses indicated an unbiased abundance estimation. The black line indicates interpolated
 785 estimates from simulation analyses with a sustained rhythm (i.e., duration = 1; see Figure 4B
 786 left). Hence, it indicates a lower bound for the abundance underestimation that occurs at low
 787 SNRs, with notable overlap with the empirical estimates in the same SNR range. **(B)** The
 788 effective rhythmic signal can be conceptualized as the background-normalized rhythmic
 789 amplitude above the background estimate (rhythmic SNR). This proxy for signal clarity is inter-
 790 individually linked to abundance estimates. **(C)** Background estimates are not consistently
 791 related to abundance. This implies that the relationship between amplitude and abundance is
 792 mainly driven by the signal, but not background amplitude (i.e., the effective signal ‘clarity’)
 793 and that associations do not arise from a misfit of the background. **(D)** Rhythmicity estimates
 794 translate between power- and phase-based definition of rhythmicity. This indicates that the
 795 BOSC-detected rhythmic spectral peak above the 1/f spectrum contains the rhythmic
 796 information that is captured by phase-based duration estimates. All data are from the resting
 797 state.

798

799 While the empirical results suggest a successful separation of rhythmic and arrhythmic
800 content at the single-trial level, we also observed strong (and stable) inter-individual differences
801 in alpha-abundance. This may imply actual differences in the duration of rhythmic engagement
802 (as indicated in Figure 6B). However, we also observed a severe underestimation of abundance
803 as a function of the overall signal-to-noise ratio (SNR) in simulations (Figure 4), thus leading
804 to the question whether empirical data fell into similar ranges where an underestimation was
805 likely. To answer this question, we calculated the individual overall SNR during the resting
806 state. We indeed observed that many overall SNRs were in the range, where simulations with
807 a stationary alpha rhythm suggested an underestimation of abundance (blue line in Figure 7A.
808 The black line indicates simulation-based estimates for stationary alpha rhythms at different
809 overall SNR levels; see section 2.8). Moreover, the coupling of individual SNR and abundance
810 values took on a deterministic shape in this range, whereas the association was reduced in
811 ranges where simulations suggest sufficient SNR for unbiased abundance estimates (orange
812 line in Figure 7A). As overall SNR is influenced by the duration of arrhythmic signal, rhythmic
813 SNR may serve as an even better predictor of abundance due to its specific relation to rhythmic
814 episodes (Figure 3). In line with this consideration, rhythmic SNR exhibited a strong linear
815 relationship to abundance (Figure 7B). Importantly, the background estimate was not
816 consistently related to abundance (Figure 7C), emphasizing that it is the ‘signal’ and not the
817 ‘noise’ component of SNR that determines detection. Similar observations were made in the
818 task data during the retention phase (Supplementary Figure 3), suggesting that this association
819 reflects a general link between the magnitude of the spectral peak and duration estimates. The
820 joint analysis of simulated and empirical data thus question the accuracy of individual duration
821 estimates, especially at low SNRs, due to the dependence of unbiased estimates on sufficient
822 rhythmic power.

823 As eBOSC defines single-trial power deviations from a stationary power threshold as a
824 criterion for rhythmicity, it remains unclear whether this association is exclusive to such a
825 ‘power thresholding’-approach or whether it constitutes a more general feature of single-trial
826 rhythmicity. To probe this question, we calculated a phase-based measure of rhythmicity,
827 termed ‘lagged coherence’ (Fransen et al., 2015), which assesses the stability of phase
828 clustering at a single sensor for a chosen cycle lag. Here, 3 cycles were chosen for comparability
829 with eBOSC’s duration threshold. Crucially, this definition of rhythmicity led to highly

830 concordant estimates with eBOSC's abundance measure³ (Figure 7D), suggesting that power-
 831 based rhythm detection above the scale-free background overlaps to a large extent with the
 832 rhythmic information captured in the phase-based lagged-coherence measure. Moreover it
 833 suggests that duration estimates are more generally coupled to rhythmic amplitudes, especially
 834 when overall SNR is low.
 835



836
 837 Figure 8: The magnitude and duration of single-trial rhythmicity are intra-individually
 838 associated. Amplitude-abundance association within subjects in the Sternberg task (1st session,
 839 all trials). Dots represent single trial estimates, color-coded by subject. (Inlay) Histogram of
 840 within-subject Fisher's z-coefficients of within-subject associations. Relationships are

³ The eBOSC duration measure was further strongly correlated with the traditional Pepisode measure (estimated at the trial-wise IAF) that results from the standard BOSC algorithm (EC: $r = .96$, $p = 2e^{-18}$; EC2: $r = .94$, $p = 2e^{-15}$; EO: $r = .97$, $p = 3e^{-20}$; EO2 = $.97$, $p = 2e^{-20}$), suggesting that both measures are similarly sensitive in our empirical data and reflect to a large extent overlapping information.

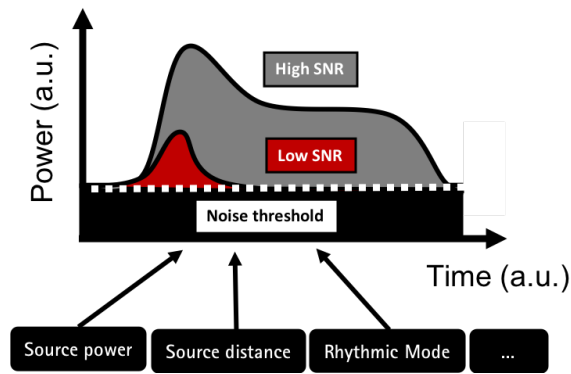
841 exclusively positive. (B) Background estimates are uncorrelated with single-trial abundance
842 fluctuations. Note that a global background is fit for each subject, channel and condition. Trial-
843 by-trial fluctuations of the background amplitude are due to (1) different backgrounds for the
844 different task conditions and (2) differences in the frequency of detected rhythmic time points.
845 The background estimate was always extracted from the frequency of the rhythmic time points
846 (see Figure 2D for a schematic example of within-episode frequency variations).

847

848 While the previous observations were made at the between-subjects level, we further
849 investigated whether such coupling also persists between trials in the absence of between-
850 person differences. In the present data, we indeed observed a positive coupling of trial-wise
851 fluctuations of rhythmic SNR and abundance (Figure 8A), whereas the estimate of the scale-
852 free background was generally unrelated to the estimated duration of rhythmicity (Figure 8B).
853 This suggests that the magnitude of ongoing power fluctuations around the stationary power
854 threshold relate to the level of estimated abundance. Figure 9 schematically shows how such an
855 amplitude-abundance coupling may be reflected in single trials as a function of rhythmic SNR.
856 These relationships were also observed in our simulations, although they were reduced in
857 magnitude at higher levels of empirical SNR (Figure 4E). Also, there was no significant
858 interindividual relationship between mean effective rhythmic SNR and the trial-wise
859 correlation magnitude ($r = -.07$; $p = .69$) in the task data. The observed between-trial association
860 in the empirical data may thus suggest an intrinsic coupling of amplitude and duration as joint
861 representations of a rhythmic mode over and above the abundance underestimation at low
862 overall SNRs.

863 In sum, these results strongly caution against the interpretation of duration measures as
864 a ‘pure’ duration metric that is independent from rhythmic power, especially at low levels of
865 SNR. The strong within-subject coupling may however also indicate an intrinsic coupling
866 between the strength and duration of neural synchrony.

867



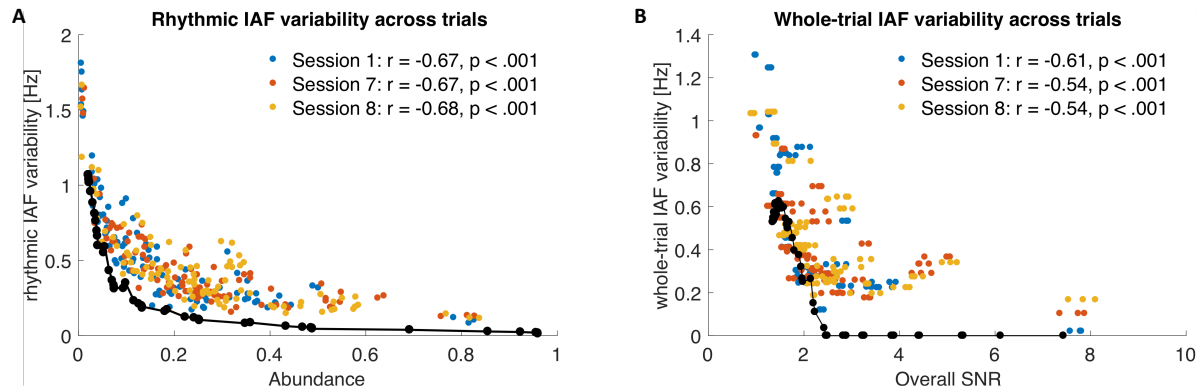
868

869 Figure 9: Schematic of the potential interdependence of rhythmic SNR and abundance. Low
 870 SNR may cause the detection of shorter supra-threshold power periods with constrained
 871 amplitude ranges, whereas prolonged periods may exceed the stationary threshold when the
 872 rhythmic signal is clearly separated from the background.

873

874 Finally, given the strong dependence of accurate duration estimates on sufficient
 875 rhythmic power, we investigated how the differences in rhythmicity affect the single-trial
 876 estimation of another characteristic, namely the individual alpha frequency (IAF) that generally
 877 shows high temporal stability (i.e., trait-qualities) within person at the average level (Grandy,
 878 Werkle-Bergner, Chicherio, Schmiedek, et al., 2013b) We observed a strong negative
 879 association between the estimated rhythmicity and fluctuations in the rhythmic IAF between
 880 trials (Figure 10A). That is, for subjects with pervasive alpha rhythms, IAF estimates were
 881 reliably stable across trials, whereas frequency estimates varied when rhythmicity was low.
 882 Notably a qualitatively and quantitatively similar association was observed in simulations with
 883 a stationary alpha frequency (black lines in Figure 10), suggesting that such variation may be
 884 artefactual. As lower abundance implies a smaller number of samples from which the IAF is
 885 estimated, this effect could amount to a sampling confound. However, we observed a similar
 886 link between overall SNR and IAF variability when the latter was estimated across all
 887 timepoints in a trial (Figure 10B). Again, simulations with stationary 10 Hz rhythms gave rise
 888 to similar results, suggesting that estimated frequency fluctuations can arise (at least in part)
 889 from the absence of clear rhythmicity. Hence, even when the IAF is intra-individually stable,
 890 its moment-to-moment estimation may induce variability when the rhythms are not clearly
 891 present.

892



893

894 Figure 10: Trial-by-trial IAF variability is associated with sparse rhythmicity. **(A)** Individual
 895 alpha frequency (IAF) precision across trials is related to abundance. Lower individual
 896 abundance estimates are associated with increased across-trial IAF variability. **(B)** This
 897 relationship also exists when considering overall SNR and IAF estimates from across the whole
 898 trial. Superimposed black lines show the 6th order polynomial fit for simulation results
 899 encompassing varying rhythm durations and amplitudes. Empirically estimated frequency
 900 variability is quantitatively similar to the bias observed at low SNRs in the simulated data.

901

902 Combined, these results suggest that the efficacy of an accurate single-trial
 903 characterization of neural rhythms relies on sufficient individual rhythmicity and can not only
 904 constrain the validity of duration estimates, but broadly affect a range of rhythm characteristics
 905 that can be inferred from single trials.

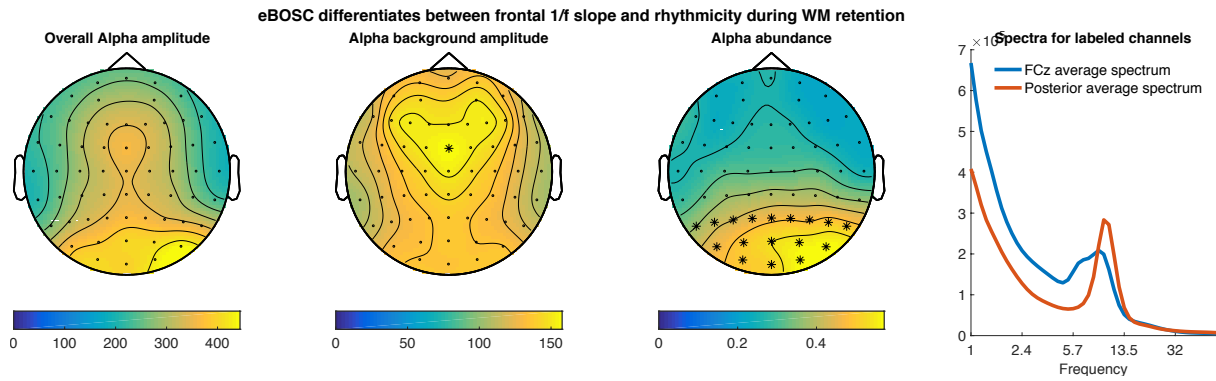
906

907 3.4 Exemplary benefits of single-trial rhythm detection: dissociation of 1/f slope and
 908 rhythmicity; rhythm-conditional spectra; characterizing sustained rhythms and transients

909

910 From the joint assessment of detection performance in simulated and empirical data, it
 911 follows that low SNR constitutes a severe challenge for single trial rhythm characterization.
 912 However, while the magnitude of rhythmicity at the single trial level constrains the detectability
 913 of rhythms, abundance represents a lower bound on rhythmic duration due to eBOSC’s high
 914 specificity. This allows the interpretation of rhythm-related metrics for those time points where
 915 rhythmicity is indicated, leading to tangible benefits over standard analyses. In this section, we
 916 present multiple proof-of-concept use cases of such benefits.

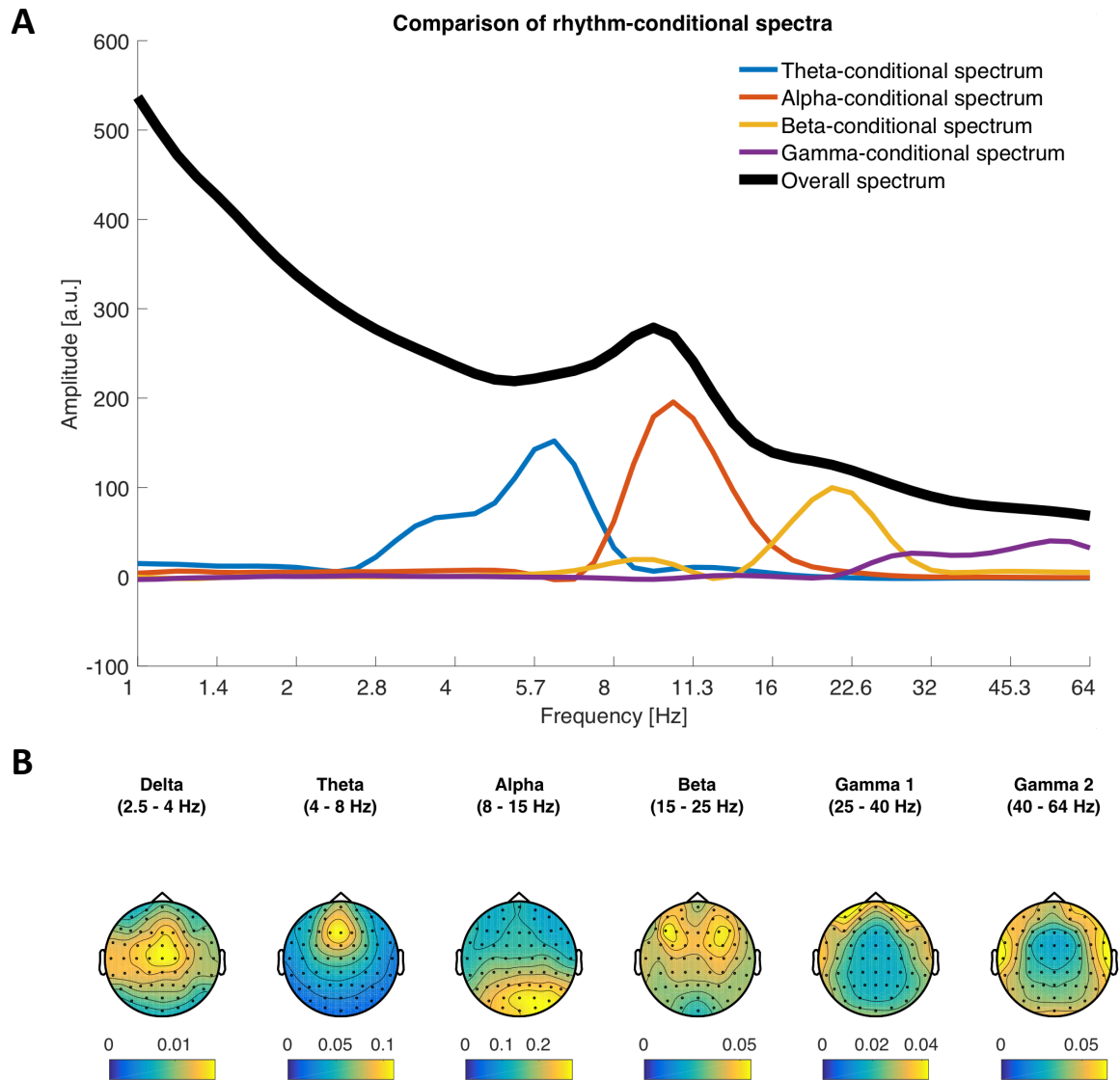
917



918
 919 Figure 11: eBOSC uncouples spatially varying topographies of rhythmic and arrhythmic power
 920 during working memory retention. Asterisks mark the channels that were selected for the
 921 spectra on the right. The topographies are grand averages from the retention phase of the
 922 Sternberg task across Sessions 1, 7 and 8.

923
 924 A considerable problem in standard narrowband power analyses is the superposition of
 925 rhythmicity on top of a scale-free $1/f$ background, effectively mixing the two components in
 926 traditional power estimates (e.g. Haller et al., 2018). In contrast, eBOSC inherently uncouples
 927 the two signals via explicit modelling of the arrhythmic background. Figure 11 presents a
 928 comparison between the standard narrowband estimate and eBOSC's background and
 929 rhythmicity metrics for the alpha band during working memory retention. While high
 930 narrowband power is observed in frontal and parietal clusters, eBOSC differentiated a frontal
 931 $1/f$ component and a posterior-occipital rhythm cluster. Identical comparisons within multiple
 932 low-frequency ranges suggest the separation of a stationary $1/f$ topography and spatially
 933 varying superpositions of rhythmicity (Supplementary Figure 4). This highlights a successful
 934 separation of the scale-free slope magnitude from rhythmicity across multiple frequencies, even
 935 when topographies are partially overlapping as in the case of theta.

936

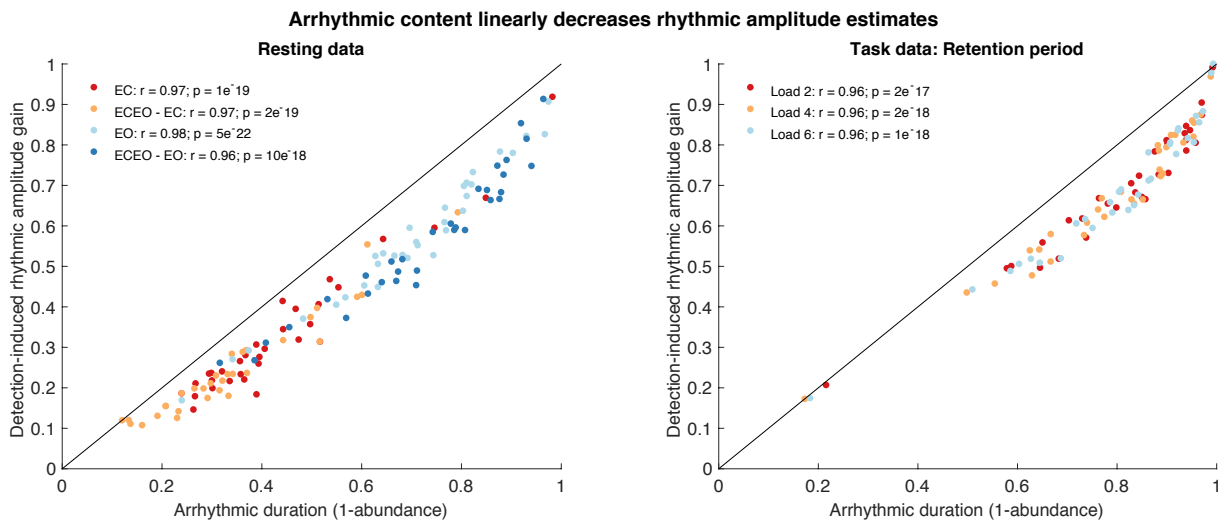


937

938 Figure 12: Time-wise indication of rhythmicity affords the analysis of rhythm-conditional
 939 spectra. (A) Comparison of rhythm-conditional spectra with the standard overall spectrum
 940 during the memory retention phase. Rhythm-conditional spectra are created by comparing
 941 spectra from time-points where a rhythm in the respective frequency range has been indicated
 942 with those where no rhythm was present. Notably, this indicates rhythmic peaks at the
 943 frequencies of interest that are not observed in the overall spectrum (e.g. theta, beta) due to the
 944 prevalence of non-rhythmic events. Simultaneous peaks beyond the target frequencies indicate
 945 cross-spectral coupling. Note that these spectra also suggest sub-clusters of frequencies (e.g. an
 946 apparent split of the ‘theta-conditional’ spectrum into a putative delta and theta component).
 947 Data are averaged across sessions, loads, subjects and channels. (B) Abundance topographies
 948 of the observed rhythm-conditional spectral peaks.

949
 950
 951
 952
 953
 954
 955
 956
 957
 958
 959
 960
 961
 962
 963
 964
 965

Furthermore, the presence of a rhythm is a fundamental assumption for the interpretation of rhythm-related metrics, i.e., like phase (Aru et al., 2015). This is often verified by observing a spectral peak at the frequency of interest. However, sparse single-trial rhythmicity may not produce an overt peak in the average spectrum due to the high prevalence of low-power arrhythmic content. Crucially, knowledge about the temporal occurrence of rhythms in the ongoing signal can be used to investigate the spectral content that is specific to those time points, thereby creating ‘rhythm-conditional spectra’. Figure 12A highlights that such rhythm-conditional spectra can recover spectral peaks for multiple canonical frequency bands, even when no clear peak is observed in the grand average spectrum. This showcases that a focus on detected rhythmic time points allows the interpretation of rhythm-related parameters. Abundance topographies for the different peaks observed in the rhythm-conditional spectra, were in line with the canonical separation of these frequencies in the literature (Figure 12B). Notably, while some rhythmicity was identified in higher frequency ranges, the associated abundance topographies suggests a muscular generator rather than a neural origin for these events.



966
 967
 968
 969
 970
 971
 972
 973

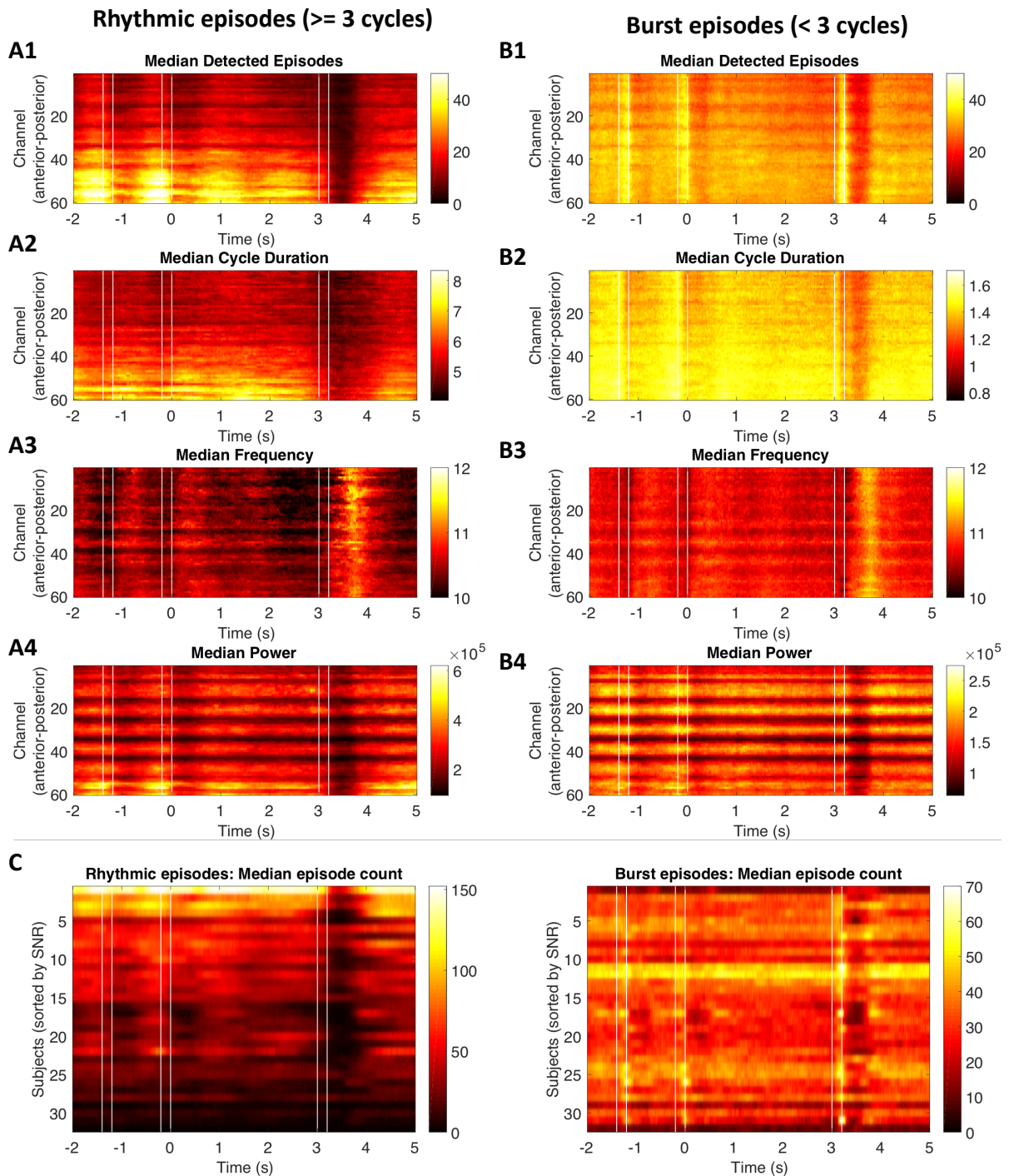
Figure 13: Arrhythmic duration linearly biases traditional power estimates during both rest (A) and task (B) states. The relative gain in alpha amplitudes from global intervals to eBOSC’s rhythmic periods (see schematic in Figure 1A and Figure 3A) increases with the arrhythmic duration in the investigated period. That is, if high arrhythmic duration was indicated, a focus on rhythmic periods strongly increased amplitudes by excluding the pervasive low-amplitude arrhythmic periods. In contrast, amplitude estimates were similar when arrhythmicity was low and hence rhythm-unspecific metrics contained little arrhythmic bias. Dots represent individual

974 condition averages during the resting state. Amplitude gain is calculated as the relative change
975 in rhythmic amplitude from the unspecific ‘overall’ amplitude (i.e., (rhythmic amplitude-
976 overall amplitude)/rhythmic amplitude). For both rhythmic and arrhythmic amplitudes, only
977 the amplitude above the background estimate was considered.

978

979 Related to the recovery of spectral amplitudes from ‘overall amplitudes’, a central
980 prediction of the present work was that the change from overall to rhythmic amplitudes (i.e.,
981 rhythm-specific gain; see Figure 3 for a schematic) scales with the presence of arrhythmic
982 signal. Stated differently, if most of the overall signal is rhythmic, the difference between
983 overall and rhythm-specific amplitude estimates should be minimal. Conversely, if the overall
984 signal consists largely of arrhythmicity, rhythm-specific amplitude estimates should strongly
985 increase from their unspecific counterparts. In line with these expectations, we observed a
986 positive, highly linear, relationship between a subject’s estimated duration of arrhythmicity and
987 the rhythm-specific amplitude gain (Figure 13). Thus, for subjects with short rhythmicity,
988 rhythm-specific amplitudes were strongly increased from overall amplitudes, whereas
989 differences were minute for subjects with prolonged rhythmicity. Note however that in the case
990 of inter-individual collinearity of amplitude and abundance (as is observed in the present data)
991 the rhythm-specific gains are unlikely to change the rank-order of subjects as the relative gain
992 will not only be proportional to the abundance, but due to the collinearity also to the original
993 amplitude. While such collinearity was high in the alpha band, decreased amplitude-abundance
994 relationships were observed for other canonical frequency bands (Supplementary Figure 5),
995 where such ‘amplitude recovery’ may have the most immediate benefits.

996

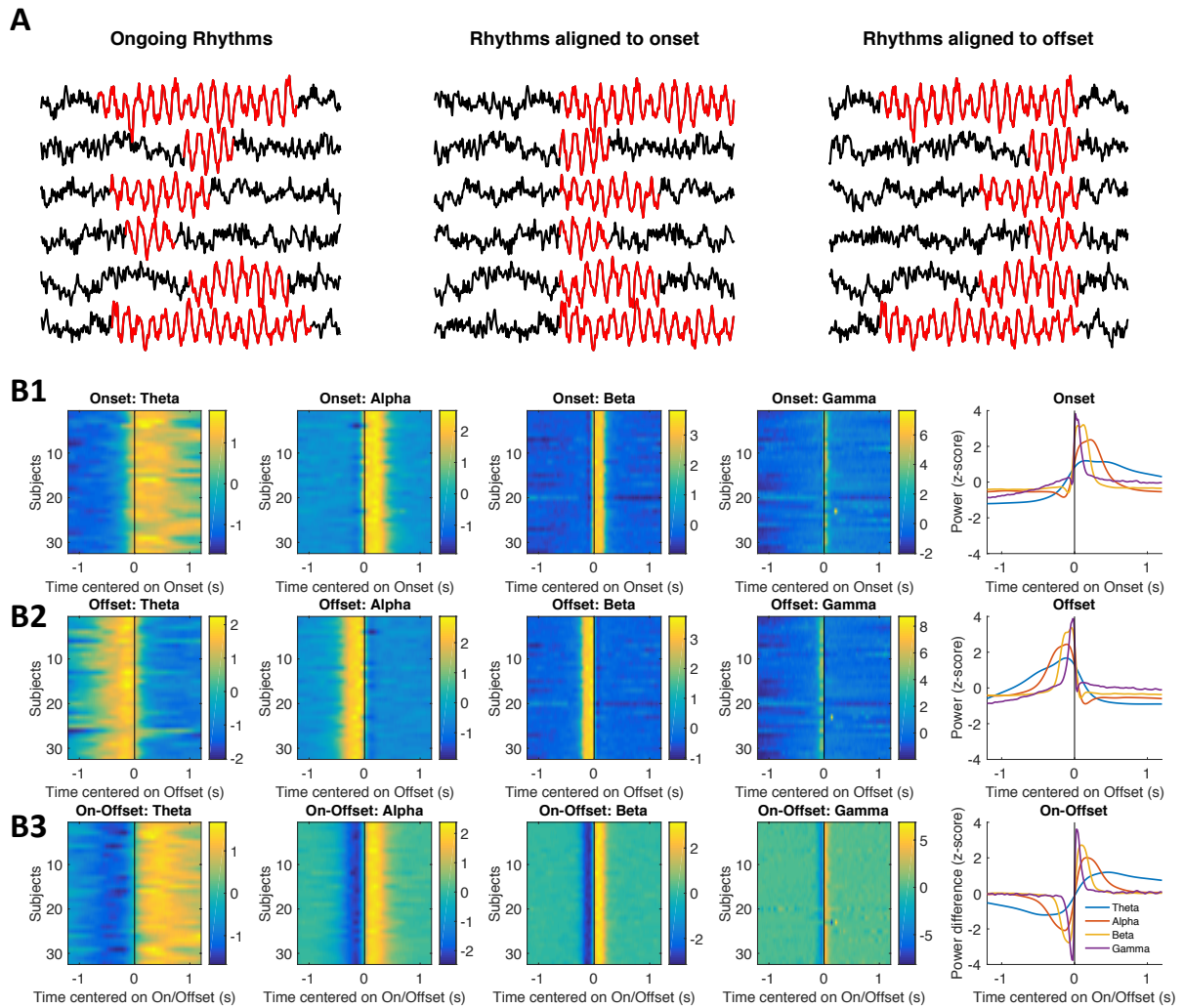


997
 998 Figure 14: eBOSC provides a varied characterization of duration-specific frequency content,
 999 separating sustained rhythmicity (A) from transients (B). Here, episodes with a mean frequency
 1000 between 8 and 15 Hz were post-hoc sorted by falling below or above a 3-cycle duration
 1001 threshold. For each index, estimates were averaged across all episodes at any time point,
 1002 followed by averaging across sessions and subjects. Note that all indices are based on episodes
 1003 that fulfil the power threshold for rhythmicity. There are notable differences (e.g., an increased
 1004 prevalence of transient events upon stimulus onset: B1 vs. A1). Furthermore, we observe

1005 frequency increases during the response period, which may relate to motor suppression. (C)
 1006 Whereas SNR posed a major constraint on the identification of sustained rhythmicity, it did not
 1007 constrain the number of detected transients, suggesting separable sources.

1008

1009 Furthermore, eBOSC's creation of continuous temporal 'episodes' affords a
 1010 characterization of rhythmic and transient episodes with significant spectral power in the
 1011 absence of an *a priori* duration requirement. Using the traditional 3-cycle threshold as a post-
 1012 hoc criterion, we observed differences in the temporal prevalence of transient events and
 1013 sustained rhythms, with a larger number of transient events following stimulus onsets, in line
 1014 with the observations made for rhythmic vs. arrhythmic power (Figure 6A6). In addition, these
 1015 episodes can be further characterized in terms of their average cycle duration (Figure 14A2,
 1016 Figure 14B2) and frequency (Figure 14A3, Figure 14B3). The latter exhibits transient increases
 1017 around the response period, likely related to motor inhibition. Notably, while overall SNR
 1018 constrains the detection of sustained rhythmicity (e.g., Figure 4A, 7A), the same was not
 1019 observed for the number of transient episodes (Figure 14C), thereby suggesting differential
 1020 origins of these signal contributions.



1021
 1022 Figure 15: On- and offsets of rhythmic episodes characterize ‘rhythm-evoked’ effects. (A)
 1023 Schematic alignment of data to the on- and offsets of rhythmic periods. (B) Rhythm on- and
 1024 offsets are marked by sudden power shifts at their respective frequency. Individual normalized
 1025 wavelet power shows a strong increase at the rhythmic onset (B1) and a decrease once rhythmic
 1026 episodes end (B2). The difference between on- and offset-related power summarizes the evoked
 1027 effect of rhythmic episodes on ongoing power (B3). Power was extracted within a fixed peri-
 1028 onset and peri-offset window for all channels where episodes were detected and subsequently
 1029 averaged across episodes, loads and channels. Finally, the individual averages were z-
 1030 normalized. The rightmost plots show the grand average across subjects. Data are from
 1031 extended periods of the Sternberg task in Session 1.

1032
 1033 Finally, the temporal specificity of spectral episodes also enables a characterization of
 1034 rhythm-‘evoked’ events. Whereas an assessment of evoked effects has thus far only been
 1035 possible with regard to external event markers, the indication of rhythm on- and offsets allows

1036 an investigation of concurrent changes that are time-locked to rhythmic events (Figure 15A).
 1037 Here, we exemplarily show that the on- and offsets of rhythmic episodes are associated with
 1038 concurrent power increases and decreases respectively (Figure 15B), adding further evidence
 1039 for the high temporal specificity of indicated on- and offsets of rhythmic episodes.

1040 In sum, these proof-of-concept applications suggest that explicit rhythm detection may
 1041 provide tangible benefits over traditional narrowband analyses due to its specific separation of
 1042 rhythmic and arrhythmic periods, despite the high collinearity of abundance and power that we
 1043 observed in the alpha band.

1044

1045 4. Discussion

1046

1047 In the present manuscript, we explored the feasibility of characterizing neural rhythms
 1048 at the level of single trials. To achieve this goal, we extended a previously published rhythm
 1049 detection method, BOSC (Whitten et al., 2011). Based on simulations we demonstrate that our
 1050 extended BOSC (eBOSC) algorithm performs well and increases detection specificity.
 1051 Crucially, the reliance on robust regression in conjunction with removal of the rhythmic power
 1052 band effectively decoupled estimation of the noise background from the rhythmic signal
 1053 component (as reflected in the divergent associations with rhythmicity estimates). In real data,
 1054 we can successfully separate rhythmic and arrhythmic, sometimes transient components, and
 1055 further characterize e.g., their amplitude, duration and frequency. In total, single-trial
 1056 characterization of neural rhythms appears promising for improving a mechanistic
 1057 understanding of rhythmic processing modes during rest and task.

1058 However, the simulations also reveal challenges for accurate rhythm characterization in
 1059 that the abundance estimates clearly depend on rhythmic power. The comparison to a phase-
 1060 based rhythm detection further suggests that this a general limitation independent of the chosen
 1061 detection algorithm. Below, we will discuss the potential and challenges of single-trial rhythm
 1062 detection in more detail.

1063

1064 4.1 The utility and potential of rhythm detection

1065

1066 Single-trial analyses are rapidly gaining importance (Jones, 2016; Stokes & Spaak,
 1067 2016), in part due to a debate regarding the sustained vs. transient nature of neural rhythms that
 1068 cannot be resolved at the level of data averages (Jones, 2016; van Ede et al., 2018). In short,
 1069 due to the non-negative nature of power estimates, time-varying transient power increases may

1070 be represented as sustained power upon averaging, indicating an ambiguity between the
1071 duration and power of rhythmic events (cf., Figure 3B). Importantly, sustained and transient
1072 events may differ in their neurobiological origin (Sherman et al., 2016), indicating high
1073 theoretical relevance for their differentiation. Moreover, many analysis procedures, such as
1074 phase-based functional connectivity, assume that estimates are directly linked to the presence
1075 of rhythmicity, therefore leading to interpretational difficulties when it is unclear whether this
1076 condition is met (Aru et al., 2015; Muthukumaraswamy & Singh, 2011). Clear identification of
1077 rhythmic time periods in single trials is necessary to resolve these issues. In the current study,
1078 we extended a state-of-the-art rhythm detection algorithm, and systematically investigated its
1079 ability to characterize the power and duration of neural alpha rhythms at the single-trial level
1080 in scalp EEG recordings.

1081 While the standard BOSC method provides a sensible detection of rhythmic activity in
1082 empirical data (Caplan et al., 2015; Whitten et al., 2011), its' ability to detect rhythmicity and
1083 disambiguate rhythmic power and duration has not yet been investigated systematically.
1084 Furthermore, we introduced multiple changes that aimed to create rhythmic episodes with a
1085 time-point-wise indication of rhythmicity. For these reasons, we assessed the performance of
1086 both algorithms in simulations. We observed that both algorithms were able to approximate the
1087 duration of rhythmicity across a large range of simulated amplitudes and durations. However,
1088 standard BOSC systematically overestimated rhythmic duration (Figure 4A). Furthermore, we
1089 observed a bias of rhythmicity on the estimated background (Figure 4C) as also noted by Haller
1090 et al. (2018). In contrast, eBOSC accounts for these problems by introducing multiple changes:
1091 First, by excluding the rhythmic peak prior to fitting the arrhythmic background, eBOSC
1092 decreased the bias of narrow-band rhythmicity on the background fit (Figure 4C), thereby
1093 effectively uncoupling the estimated background amplitude from the indicated rhythmicity
1094 (Figure 7C, 8B). Second, the post-processing of detected segments provided a more specific
1095 characterization of neural rhythms compared to standard BOSC (Figures 4). In particular,
1096 accounting for the temporal extension of the wavelet (Figure 2) increased the temporal
1097 specificity of rhythm detection as indicated by a better adherence to the *a priori* duration
1098 threshold along with more precise duration estimates. In contrast to the high specificity, the
1099 algorithm did trade off sensitivity, leading to sensitivity losses especially at low SNR. The
1100 dependence on accurate duration estimation on sufficient SNR more generally caused problems
1101 for empirically disentangling rhythmic power and duration that we discuss in more detail in
1102 section 4.2. In sum, the simulations highlight that eBOSC provides a sensible differentiation of
1103 rhythmic and arrhythmic time points as well as accurate duration estimates, but also highlight

1104 challenges that arise from sensitivity problems when the magnitude of rhythms is low. In
 1105 empirical data, eBOSC likewise led to a sensible separation of rhythmic from arrhythmic
 1106 topographies (Figure 5A, Figure 11, Supplementary Figure 4) and time courses, both at the
 1107 average (Figure 6A) and the single-trial level (Figure 6B). This suggests a sensible separation
 1108 of rhythmic and arrhythmic time points also in empirical scenarios.

1109 The specific separation of rhythmic and arrhythmic time points has multiple immediate
 1110 benefits that we validated using empirical data from resting and task states. First, eBOSC
 1111 separates the scale-free background from superimposed rhythmicity in a principled manner.
 1112 The theoretical importance of such separation has previously been highlighted (Haller et al.,
 1113 2018), as narrow-band estimates traditionally confound the two signals. Here, we show that
 1114 such a separation empirically produces different topographies for the arrhythmic background
 1115 and the superimposed rhythmicity (Figure 11 and Supplementary Figure 4). In line with these
 1116 findings, Caplan et al. (2015) described a rhythmic occipital alpha topography, whereas overall
 1117 power included an additional anterior component across multiple lower frequencies. While that
 1118 study did not plot topographies for the background estimates, our study suggests that this frontal
 1119 component is captured by the background magnitude. This provides convergent evidence for a
 1120 principled separation of rhythmic and arrhythmic spectral content which may be treated as a
 1121 signal of interest in itself (Buzsáki & Mizuseki, 2014; He et al., 2010).

1122 The separation of these signal sources at single time points can further be used to
 1123 summarize the rhythmic single-trial content via rhythm-conditional spectra (Figure 12).
 1124 Crucially, such a focus on rhythmic periods resolves biases from arrhythmic periods in the
 1125 segments of interest. In line with our hypotheses, simulations (Figure 3B) and empirical data
 1126 (Figure 13) indicate that arrhythmic episodes in the analysed segment bias overall power
 1127 estimates relative to the extent of their duration. Conversely, a focus on rhythmic periods
 1128 induces the most pronounced amplitude gains when rhythmic periods are sparse. This is in line
 1129 with previous observations by Cole & Voytek (2018), showing dissociations between power
 1130 and frequency estimates when considering ‘rhythmic’ vs. unspecific periods and extend those
 1131 observations by showing a strong linear dependence between the rhythm-specific change in
 1132 estimates and the duration of arrhythmic bias (Figure 13).

1133 Moreover, by allowing a post-hoc duration threshold, eBOSC can disentangle transient
 1134 and sustained events in a principled manner (Figure 14). This may provide new insights into
 1135 the contribution of different biophysical signal generators (Sherman et al., 2016) to observed
 1136 neural dynamics and aid the characterization of these processes. Such characterization includes
 1137 multiple parameters, such as the frequency of rhythmic episodes, their duration, their amplitude

1138 and other indices that we did not consider here (e.g., instantaneous phase, time domain shape).
1139 Here, we observed an increased number of alpha transients following stimulus onsets, and more
1140 sustained rhythms when no stimulus was presented (Figure 6A, Figure 14). In line with these
1141 observations, Peterson & Voytek (2017) recently proposed alpha ‘bursts’ to increase visual gain
1142 during stimulus onsets and contrasted this role with decreased cortical processing during
1143 sustained alpha rhythms. Our data supports such a distinction between sustained and transient
1144 events, although it should be noted that the present transients likely reflect time-domain
1145 deflections that are resolved at alpha frequency and may therefore not directly relate to the
1146 ‘rhythmic bursts’ proposed by Peterson & Voytek (2017). Note that the reported duration of
1147 ‘burst’ events in the literature is still diverse, often exceeding the 3-cycle threshold used here
1148 (Peterson & Voytek, 2017). In contrast to eBOSC however, previous work has not accounted
1149 for the impact of wavelet duration. It is thus conceivable that power transients that were
1150 previously characterized as 3 cycles or longer are actually shorter after correcting for the impact
1151 of wavelet convolution, as is done in the current eBOSC implementation (Figure 2). This
1152 temporal specificity also allows an indication of rhythm-evoked changes, here exemplified with
1153 respect to rhythm-evoked power changes (Figure 15). We observed a precise and systematic
1154 time-locking of power changes to the on- and offset of detected rhythmic episodes. This further
1155 validates the detection assumptions of the eBOSC method (i.e. significant power increases from
1156 the background), and highlights the temporal specificity of eBOSC’s rhythmic episodes.

1157 In total, eBOSC’s single-trial characterization of neural rhythms provides multiple
1158 immediate benefits over traditional average-based analyses temporally precise indication of
1159 rhythmic and arrhythmic periods. It thus appears promising for improving a mechanistic
1160 understanding of rhythmic processing modes during rest and task.

1161

1162 4.2 Single-trial detection of rhythms: rhythmic SNR as a central challenge

1163

1164 The aforementioned examples highlight the utility of differentiating rhythmic and
1165 arrhythmic periods in the ongoing signal. However, the simulations also indicated problems to
1166 accurately do so when rhythmic power is low. That is, the recognition of rhythms was more
1167 difficult at low levels of SNR, leading to problems with their further characterization. In
1168 particular, our simulations suggest that estimates of the duration (Figure 7A) and frequency
1169 stationarity (Figure 10) increasingly deviate from the simulated parameters as the SNR
1170 decreases. Changes in instantaneous alpha frequency as a function of cognitive demands have
1171 been theorized and reported in the literature (Haegens, Cousijn, Wallis, Harrison, & Nobre,

1172 2014; Herrmann, Murray, Ionta, Hutt, & Lefebvre, 2016; Mierau, Klimesch, & Lefebvre, 2017;
 1173 Samaha & Postle, 2015; Wutz, Melcher, & Samaha, 2018), with varying degrees of control for
 1174 power differences between conditions and individuals. Our empirical analyses suggest an
 1175 increased trial-by-trial variability of individual alpha frequency estimates as SNR decreases
 1176 (Figure 10). Meanwhile, simulations suggest that such increased variance - both estimated
 1177 within indicated rhythmic periods and across whole trials – may result from lower SNR. While
 1178 our results do not negate the possibility of real frequency variations of the alpha rhythm with
 1179 changes in task load, they emphasize the importance of controlling for the presence of rhythms,
 1180 mirroring considerations for the interpretation of phase estimates (Muthukumaraswamy &
 1181 Singh, 2011) and amplitudes. This exemplifies how stable inter-individual differences in
 1182 rhythmicity (whether due to a real absence of rhythms or prevalent measurement noise; e.g.,
 1183 distance between source and sensor; head shape; skull thickness) can affect a variety of ‘meta’-
 1184 indices (like phase, frequency, duration) whose estimation accuracy relies on apparent
 1185 rhythmicity.

1186 The challenges for characterizing rhythms with low rhythmic power also apply to the
 1187 estimated rhythmic duration, where the issue is particularly challenging in the face of legitimate
 1188 interest regarding the relationship between the power and duration of rhythmic events. In
 1189 particular, sensitivity problems at low rhythmic magnitudes challenge the ability to empirically
 1190 disambiguate rhythmic duration and power, as it makes the former dependent on the latter in
 1191 the presence of noise (e.g., Figure 3B). Crucially, a tight link between these parameters was
 1192 also observed in the empirical data. During both rest and task states, we observed gradual and
 1193 stable inter-individual differences in the estimated extent of rhythmicity that were most strongly
 1194 related to the overall SNR in ranges with a pronounced sensitivity loss in simulations (see
 1195 Figure 5A black line). Given the observed detection problems in our simulations, this
 1196 ambiguates whether low empirical duration estimates indicate temporally constrained rhythms
 1197 or estimation problems. Conceptually, this relates to the difference between lower SNR subjects
 1198 having (A) low power, transient alpha engagement or (B) low power, sustained alpha
 1199 engagement that was too faint to be detected (i.e., sensitivity problems). While the second was
 1200 the case in the simulations, the absence of a ground truth does not allow us to resolve this
 1201 ambiguity in empirical data.

1202 Empirically, multiple results suggest that the low duration estimates at low SNRs did
 1203 not exclusively arise from idiosyncrasies of our algorithm. Notably, inter-individual differences
 1204 in eBOSC’s abundance measure were strongly correlated with standard BOSC’s Pepisode
 1205 measure (Whitten et al., 2011) as well as the phase-based lagged coherence index (Fransen et

1206 al., 2015), thus showing high convergence with different state-of-the-art techniques (Figure
1207 7D). Furthermore, detection performance was visually satisfying in single trials given
1208 observable task-locked rhythm dynamics for rhythmic, but not arrhythmic periods (Figure 6B).
1209 Moreover, the observed relationship between amplitude gain and abundance suggests a
1210 successful exclusion of (low-power) arrhythmic episodes at the individual level (Figure 13).
1211 These observations indicate that low SNR conditions present a fundamental challenge to single-
1212 trial characterization across different methods. The convergence between power- and phase-
1213 based definitions of rhythmicity also indicates that rhythmicity can exhaustively be described
1214 by the spectral peak above the background, in line with our observations regarding rhythm-
1215 conditional spectra (Figure 12).

1216 The observation of strong between-person coupling as a function of SNR suggests that
1217 such sensitivity limitations may account for the inter-individual amplitude-abundance
1218 associations. However, we also observed a positive association between subjects with high
1219 alpha SNR. Likewise, we observed positive associations between abundance and rhythmic
1220 SNR, but not the background estimate at the within-subject level (Figure 6). While trial-wise
1221 coupling was also present in our simulations, the magnitude of these relationships were lower
1222 at high SNR (Figure 3E). Conversely, in empirical data, the within-subject association did not
1223 vary in magnitude as a function of the individual SNR. Hence, separate sources may contribute
1224 to a coupling of rhythmic amplitude and abundance: a methods-induced association in low SNR
1225 ranges and an intrinsic coupling between rhythmic strength and duration as a joint
1226 representation of rhythmic synchrony. Notably, empirical within-subject coupling between
1227 rhythmic amplitude and duration was previously described for LFP beta bursts in the
1228 subthalamic nucleus (Tinkhauser et al., 2017), with both parameters being sensitive to a drug
1229 manipulation. This association was interpreted as a “progressive synchronization of inputs over
1230 time” (Tinkhauser et al., 2017; p. 2978). Due to the absence of a dissociation of these
1231 parameters, it remains unclear whether the two measures make independent contributions or
1232 whether they can be conceptualized as a single underlying latent ‘rhythmicity’ index. To resolve
1233 this ambiguity, clear dissociations of amplitude and duration estimates in data with high
1234 rhythmic SNR are necessary. Notably, potential dissociations between the individual power and
1235 duration of beta events has been suggested by Shin et al. (2017), who described differential
1236 relationships between event number, power and duration to mean power and behaviour.

1237 The high collinearity between overall amplitude and abundance may be surprising given
1238 evidence of their potential dissociation in the case of beta bursts (where overall abundance is
1239 low, but burst amplitudes are high) (Lundqvist et al., 2016; Sherman et al., 2016; Shin et al.,

1240 2017). In line with this notion, Fransen et al. (2015) reported an increased sensitivity for central
1241 beta rhythmicity using the lagged coherence duration index compared with overall power. It
1242 may thus be that the alpha range is an outlier in this regard due to the presence of relatively
1243 sustained rhythmicity. A frequency-wise comparison of the between- and within-subject
1244 collinearity between amplitude and abundance collinearity indicated a particularly high overlap
1245 for the alpha range (Supplementary Figure 5) with relatively lower coupling for delta, theta and
1246 beta. Whether this is due to their lower rhythmicity in the current data or due to systematic
1247 differences between frequencies remains an open question and requires data with more
1248 prominent rhythmicity in these bands.

1249 The strong collinearity of amplitude and duration estimates also questions the successful
1250 disambiguation of the two indices in empirical data and more generally the interpretation of
1251 duration as an independent index. In cases where such metrics only serve as a sensitive and/or
1252 specific replacement for power (Caplan et al., 2015; Fransen et al., 2015) this may not be
1253 problematic, but care has to be taken in interpreting available duration indices as power-
1254 independent characteristics of rhythmic episodes. An independent duration index becomes
1255 increasingly important however to assess whether rhythms are stationary or transient. For this
1256 purpose, both amplitude thresholding and phase-progression criteria have been proposed (Cole
1257 & Voytek, 2018; Peterson & Voytek, 2017; Sherman et al., 2016; van Ede et al., 2018; Vidaurre,
1258 Myers, Stokes, Nobre, & Woolrich, 2018). Here, we show that both methods arrive at similar
1259 conclusions regarding individual rhythmic duration and that the mentioned challenges are
1260 therefore applicable to both approaches. As an alternative to threshold-based methods, Van Ede
1261 et al. (2018) propose methods based on e.g., Hidden Markov Models (Vidaurre et al., 2018;
1262 2016) for the estimation of rhythmic duration. These approaches are interesting as the definition
1263 of states to be inferred in single trials is based on individual (or group) averages, while the
1264 multivariate nature of the signals across channels is also taken into account. It is a viable
1265 question for future investigations whether such approaches can adequately characterize the
1266 duration of rhythmic states in scenarios where the present methods fail.

1267 Likewise, single-trial properties are gaining relevance in decoding analyses that
1268 traditionally operate with few if any trial averages. Depending on whether the relevant feature
1269 vectors include neural rhythms, differences in rhythmicity may therefore also affect decoding
1270 feasibility. Recently, large inter-individual differences in decoding performance have been
1271 observed (Westner, Dalal, Hanslmayr, & Staudigl, 2018), and it remains an intriguing question
1272 whether such decoding efficacy covaries with the extent of rhythmicity. By characterizing a
1273 recording's rhythmicity, eBOSC provides a tool to investigate such putative links.

1274

1275 4.3 Comparison to other single-trial detection algorithms & limitations

1276

1277 The BOSC-family of methods is conceptually similar to other methods that are currently
1278 used to identify and describe spectral events in single trials. These methods share the underlying
1279 principle of identifying rhythmic events based on momentary power increases relative to an
1280 average baseline. Such detection is most common regarding transient beta bursts, for which a
1281 beta-specific power threshold is often defined. For example, Sherman et al. (2016) identified
1282 transient beta events based on the highest power within the beta range, i.e., without an explicit
1283 threshold. Shin et al. (2017) introduced a beta-specific power threshold based on average pre-
1284 stimulus power. Similarly, Feingold et al. (2015) defined beta events as exceeding 1.5/3 times
1285 the median beta power of that channel, while Tinkhauser et al. (2017) applied a 75th percentile
1286 threshold to beta amplitudes. These approaches therefore use a spectrally local power criterion,
1287 but no duration threshold. Most closely related to the BOSC-family is the MODAL method by
1288 Watrous et al. (2018), which similarly uses a robust fit of the 1/f spectrum to detect rhythmic
1289 events in continuous data and then further derives frequency and phase estimates for those
1290 rhythmic periods. This is conceptually similar to eBOSC's definition as 'statistically
1291 significant' deviations in power from the 1/f background spectrum, except for the absence of a
1292 dedicated power or duration threshold. However, all of the above methods share the
1293 fundamental assumption of a momentary power deviation from a frequency-specific
1294 'background', with varying implementations of a 1/f model assumption. Such assumption can
1295 be useful to avoid a bias of rhythmic content on the power threshold (as a spectrally local power
1296 threshold depends on the average magnitude of band-limited rhythmicity, i.e., arrhythmic +
1297 rhythmic power). Removing the rhythmic peak prior to background modelling helps to avoid
1298 such bias (Figure 4C). The eBOSC method thereby provides a principled approach for the
1299 detection of single-trial events across frequencies (as shown in Figure 12).

1300 A systematic and general removal of spectral peaks remains a challenge for adequate
1301 background estimates. In the current application, we exclusively removed alpha-band power
1302 prior to performing the background fit. While the alpha rhythm produced the largest spectral
1303 peak in our data (see Supplementary Figure 2), this should not be understood as a fixed
1304 parameter of the eBOSC approach, as other rhythmic peaks may bias the estimation of the
1305 background spectrum depending on the recording's specifics (e.g., type, location etc.). We

1306 perceive the need to remove rhythmic peaks prior to background fitting as a general one⁴, as
 1307 residual spectral peaks bias detection efficacy across the entire spectrum via misfits of the
 1308 background intercept and/or slope. In particular, rhythmic peaks at higher frequencies
 1309 disproportionally increase the background estimate at lower frequencies due to the fitting in
 1310 logarithmic space. Thus, a principled removal of *any* spectral peaks in the average spectrum is
 1311 necessary. Recently, Haller et al. (2018) proposed a principled approach for the removal of
 1312 rhythmic spectral peaks, which may afford rhythm-unbiased background estimates without
 1313 requiring priors regarding the location of spectral peaks. It may thus represent a useful pre-
 1314 processing step for further applications. Regarding the present data, we anticipate no qualitative
 1315 changes compared to our alpha exclusion approach as (a) we did not observe an association
 1316 between background and rhythmicity estimates (Figure 7, 8), and the signal was dominated by
 1317 an alpha frequency peak, which consistently exceeded eBOSC's power threshold
 1318 (Supplementary Figure 2).

1319 Our results further question the adequacy of a stationary power threshold (as
 1320 traditionally employed and used here) for assessing the amplitude-duration relationship
 1321 between individual rhythmic episodes. In our empirical analyses, the rhythmic SNR, reflecting
 1322 the deviation of amplitudes during rhythmic periods from the stationary background, was
 1323 consistently most strongly associated with the estimated duration (Figure 7 & 8). While keeping
 1324 the background (and thus the power threshold) stable conforms with the common assumption
 1325 of rhythmicity being captured within a spectral peak deviating from a stationary background
 1326 (Figure 12), it may also exacerbate an amplitude-abundance coupling on a trial-by-trial basis
 1327 (see Figure 9 for a schematic of the assumed association) as ongoing power fluctuations can
 1328 only be explained by changes in the rhythmic and not the arrhythmic power term. Further
 1329 research on dynamic thresholds may shed further light on this issue.

1330 Another point worth highlighting is that eBOSC operates on wavelet-derived power
 1331 estimates. The specific need for wavelet estimates results from model-based assumptions about
 1332 the time-frequency extension of the wavelet that are used for refining detected rhythmic time
 1333 points (see Figure 2 and section 2.6). Naturally, the choice of wavelet parameters, specifically
 1334 their center frequency and duration, influences the time-frequency representations upon which
 1335 eBOSC operates. Here, we used 6 cycles as the duration parameter, in line with previous work
 1336 with standard BOSC (Caplan et al., 2015; Whitten et al., 2011). In a supplementary analysis,

⁴ A potential bias is less likely in the case of sporadic rhythmicity that does not produce a peak in the average spectrum. In this case, the power of the single-trial events would exceed the background estimate that is decreased due to the prevalence of arrhythmic periods.

1337 we compared detection performance using a 3 cycle wavelet and found increased accuracy only
1338 for short rhythmicity, whereas the sensitivity to longer rhythmicity was decreased
1339 (Supplementary Figure 6). This is consistent with the assumption that wavelet duration
1340 regulates the trade-off between temporal and spectral specificity, with longer wavelets allowing
1341 for a finer separation of nearby frequencies at the cost of temporal specificity. Another free
1342 parameter concerns the choice of center frequencies. In the post-processing procedures, we
1343 perform a sort of spectral filtering based on the pass-band of the wavelet (Figure 2), which is
1344 determined by its duration. Resolving rhythms at nearby frequencies thus requires the use of
1345 wavelets with sufficient frequency resolution, not only with regard to the sampled frequencies,
1346 but also a sufficient duration of the wavelet. This highlights the dependence of eBOSC outputs
1347 on the specifics of the wavelet-based transformation from the time into the frequency domain.

1348 An alternative, parallel approach to characterize ongoing rhythmicity is based on
1349 characterizing the waveform shape in the time domain, thereby circumventing power analyses
1350 entirely (Cole & Voytek, 2018). While such an approach is intriguing, further work is needed
1351 to show which analysis sequence is more fruitful: (a) identifying events in the frequency domain
1352 and then describing the associated waveform shape in the time domain (e.g., eBOSC) or (b)
1353 identifying events and characterizing them based on time domain features (e.g., cycle-by-cycle
1354 analysis). As both procedures operate on the basis of single trials, similar challenges (i.e.,
1355 especially rhythmic SNR) are likely to apply to both approaches.

1356

1357 5. Conclusion

1358

1359 We extended a state-of-the-art rhythm detection method and characterized alpha
1360 rhythms in simulated, resting and task data at the single trial level. By using simulations, we
1361 show that rhythm detection can be employed to derive specific estimates of rhythmicity, with
1362 fine-grained control over its definition, and to reduce the bias of rhythm duration on amplitude
1363 estimates that commonly exists in standard analysis procedures. However, we also observe
1364 striking inter-individual differences in the indicated duration of rhythmicity, which for subjects
1365 with low alpha power may be due to insufficient single-trial rhythmicity. We further show that
1366 low rhythmicity can lead to biased estimates, in particular underestimated duration and
1367 increased variability of rhythmic frequency. Given these constraints, we have provided
1368 examples of eBOSC's efficacy to characterize rhythms that may prove useful for investigating
1369 the origin and functional role of neural rhythms in health and disease, and in turn, the current
1370 study works to establish the foundation for ideographic analyses of neural rhythms.

1371

1372 *Data availability*

1373

1374 The scripts implementing the eBOSC pipelines are available at github.com/jkosciessa/eBOSC
1375 alongside the simulation scripts that were used to assess eBOSC's detection properties.

1376

1377 *Funding*

1378 This study was conducted within the project 'Cognitive and Neuronal Dynamics of Memory
1379 across the Lifespan (CONMEM)' at the Center for Lifespan Psychology, Max Planck Institute
1380 for Human Development (MPIB). MW-B's work was supported by grants from the German
1381 Research Foundation (DFG, WE 4269/3-1 and WE 4269/5-1) as well as an Early Career
1382 Research Fellowship 2017 – 2019 awarded by the Jacobs Foundation. JQK is a pre-doctoral
1383 fellow of the International Max Planck Research School on Computational Methods in
1384 Psychiatry and Ageing Research (IMPRS COMP2PSYCH). The participating institutions are
1385 the Max Planck Institute for Human Development, Berlin, Germany, and University College
1386 London, London, UK. For more information, see [https://www.mps-ucl-](https://www.mps-ucl-centre.mpg.de/en/comp2psych)
1387 [centre.mpg.de/en/comp2psych](https://www.mps-ucl-centre.mpg.de/en/comp2psych)

1388

1389 *Acknowledgements*

1390 We thank our research assistants and participants for their contributions to the present work.
1391 We thank our anonymous reviewers for their helpful comments on an earlier version of this
1392 manuscript.

1393 **References**

1394

1395 Aru, J., Aru, J., Priesemann, V., Wibral, M., Lana, L., Pipa, G., et al. (2015). Untangling
1396 cross-frequency coupling in neuroscience., *31*, 51–61.

1397 <http://doi.org/10.1016/j.conb.2014.08.002>

1398 Atallah, B. V., & Scanziani, M. (2009). Instantaneous Modulation of Gamma Oscillation
1399 Frequency by Balancing Excitation with Inhibition. *Neuron*, *62*(4), 566–577.

1400 <http://doi.org/10.1016/j.neuron.2009.04.027>

1401 Bach, M. (1996). The Freiburg Visual Acuity test--automatic measurement of visual acuity.
1402 *Optometry & Vision Science*, *73*(1), 49–53.

1403 Bach, M. (2007). The Freiburg Visual Acuity Test-variability unchanged by post-hoc re-
1404 analysis, *245*(7), 965–971. <http://doi.org/10.1007/s00417-006-0474-4>

1405 Bell, A. J., & Sejnowski, T. J. (1995). An information-maximization approach to blind
1406 separation and blind deconvolution. *Neural Computation*, *7*(6), 1129–1159.

1407 Berger, H. (1938). Über das Elektrenkephalogramm des Menschen. *Archiv Für Psychiatrie*
1408 *Und Nervenkrankheiten*, *108*(3), 407–431. <http://doi.org/10.1007/BF01824101>

1409 Brookes, M. J., Wood, J. R., Stevenson, C. M., Zumer, J. M., White, T. P., Liddle, P. F., &
1410 Morris, P. G. (2011). Changes in brain network activity during working memory tasks: A
1411 magnetoencephalography study. *NeuroImage*, *55*(4), 1804–1815.

1412 <http://doi.org/10.1016/j.neuroimage.2010.10.074>

1413 Buzsáki, G. (2006). *Rhythms of the Brain*. New York: Oxford University Press.

1414 Buzsáki, G., & Mizuseki, K. (2014). The log-dynamic brain: how skewed distributions affect
1415 network operations. *Nature Publishing Group*, *15*(4), 264–278.

1416 <http://doi.org/10.1038/nrn3687>

1417 Buzsáki, G., Anastassiou, C. A., & Koch, C. (2012). The origin of extracellular fields and
1418 currents — EEG, ECoG, LFP and spikes. *Nature Reviews Neuroscience*, *13*(6), 1–14.

1419 <http://doi.org/10.1038/nrn3241>

1420 Caplan, J. B., Bottomley, M., Kang, P., & Dixon, R. A. (2015). Distinguishing rhythmic from
1421 non-rhythmic brain activity during rest in healthy neurocognitive aging. *NeuroImage*,
1422 *112*, 341–352. <http://doi.org/10.1016/j.neuroimage.2015.03.001>

1423 Caplan, J. B., Madsen, J. R., Raghavachari, S., & Kahana, M. J. (2001). Distinct patterns of
1424 brain oscillations underlie two basic parameters of human maze learning. *Journal of*
1425 *Neurophysiology*, *86*(1), 368–380.

1426 Cohen, M. X. (2014). Analyzing neural time series data: theory and practice.

- 1427 Cohen, M. X. (2017). Where Does EEG Come From and What Does It Mean? *Trends in*
 1428 *Neurosciences*, 40(4), 208–218. <http://doi.org/10.1016/j.tins.2017.02.004>
- 1429 Cole, S. R., & Voytek, B. (2018). Cycle-by-cycle analysis of neural oscillations. *bioRxiv*,
 1430 302000. <http://doi.org/10.1101/302000>
- 1431 Feingold, J., Gibson, D. J., DePasquale, B., & Graybiel, A. M. (2015). Bursts of beta
 1432 oscillation differentiate postperformance activity in the striatum and motor cortex of
 1433 monkeys performing movement tasks. *Proceedings of the National Academy of Sciences*,
 1434 112(44), 13687–13692. <http://doi.org/10.1073/pnas.1517629112>
- 1435 Fransen, A. M. M., van Ede, F., & Maris, E. (2015). Identifying neuronal oscillations using
 1436 rhythmicity. *NeuroImage*, 118(C), 256–267.
 1437 <http://doi.org/10.1016/j.neuroimage.2015.06.003>
- 1438 Grandy, T. H., Werkle-Bergner, M., Chicherio, C., Lövdén, M., Schmiedek, F., &
 1439 Lindenberger, U. (2013a). Individual alpha peak frequency is related to latent factors of
 1440 general cognitive abilities. *NeuroImage*, 79(C), 10–18.
 1441 <http://doi.org/10.1016/j.neuroimage.2013.04.059>
- 1442 Grandy, T. H., Werkle-Bergner, M., Chicherio, C., Schmiedek, F., Lövdén, M., &
 1443 Lindenberger, U. (2013b). Peak individual alpha frequency qualifies as a stable
 1444 neurophysiological trait marker in healthy younger and older adults. *Psychophysiology*,
 1445 50(6), 570–582. <http://doi.org/10.1111/psyp.12043>
- 1446 Grandy, T., Lindenberger, U., & Werkle-Bergner, M. (2017). When group means fail: Can
 1447 one size fit all? *bioRxiv*. <http://doi.org/10.1101/126490>
- 1448 Gross, J. (2014). Analytical methods and experimental approaches for electrophysiological
 1449 studies of brain oscillations. *Journal of Neuroscience Methods*, 228, 57–66.
 1450 <http://doi.org/10.1016/j.jneumeth.2014.03.007>
- 1451 Grossmann, A., & Morlet, J. (1985). Decomposition of functions into wavelets of constant
 1452 shape, and related transforms. In L. Streit (Ed.), *Mathematics 1 Physic* (pp. 135–165).
 1453 Singapore: World Scientific.
- 1454 Haegens, S., Cousijn, H., Wallis, G., Harrison, P. J., & Nobre, A. C. (2014). Inter- and intra-
 1455 individual variability in alpha peak frequency. *NeuroImage*, 92(C), 46–55.
 1456 <http://doi.org/10.1016/j.neuroimage.2014.01.049>
- 1457 Haller, M., Donoghue, T., Peterson, E., Varma, P., Sebastian, P., Gao, R., et al. (2018).
 1458 Parameterizing neural power spectra. *bioRxiv*, 1–16. <http://doi.org/10.1101/299859>
- 1459 Hansen, E. W. (2014). DFT Properties and Theorems. In *Fourier transforms. Principles and*
 1460 *applications* (p. 128). Hoboken, New Jersey: John Wiley & Sons.

- 1461 He, B. J., Zempel, J. M., Snyder, A. Z., & Raichle, M. E. (2010). The temporal structures and
 1462 functional significance of scale-free brain activity. *Neuron*, *66*(3), 353–369.
 1463 <http://doi.org/10.1016/j.neuron.2010.04.020>
- 1464 Herrmann, C. S., Murray, M. M., Ionta, S., Hutt, A., & Lefebvre, J. (2016). Shaping Intrinsic
 1465 Neural Oscillations with Periodic Stimulation. *The Journal of Neuroscience : the Official*
 1466 *Journal of the Society for Neuroscience*, *36*(19), 5328–5337.
 1467 <http://doi.org/10.1523/JNEUROSCI.0236-16.2016>
- 1468 Holland, P. W., & Welsch, R. E. (2007). Robust regression using iteratively reweighted least-
 1469 squares. *Communications in Statistics - Theory and Methods*, *6*(9), 813–827.
 1470 <http://doi.org/10.1080/03610927708827533>
- 1471 Jensen, O., Gelfand, J., Kounios, J., & Lisman, J. E. (2002). Oscillations in the alpha band (9-
 1472 12 Hz) increase with memory load during retention in a short-term memory task.
 1473 *Cerebral Cortex*, *12*(8), 877–882.
- 1474 Jokisch, D., & Jensen, O. (2007). Modulation of gamma and alpha activity during a working
 1475 memory task engaging the dorsal or ventral stream. *The Journal of Neuroscience : the*
 1476 *Official Journal of the Society for Neuroscience*, *27*(12), 3244–3251.
 1477 <http://doi.org/10.1523/JNEUROSCI.5399-06.2007>
- 1478 Jones, S. R. (2016). When brain rhythms aren't 'rhythmic': implication for their mechanisms
 1479 and meaning. *Current Opinion in Neurobiology*, *40*, 72–80.
 1480 <http://doi.org/10.1016/j.conb.2016.06.010>
- 1481 Klimesch, W. (2012). alpha-band oscillations, attention, and controlled access to stored
 1482 information. *Trends in Cognitive Sciences*, *16*(12), 606–617.
 1483 <http://doi.org/10.1016/j.tics.2012.10.007>
- 1484 Linkenkaer-Hansen, K., Nikouline, V. V., Palva, J. M., & Ilmoniemi, R. J. (2001). Long-
 1485 range temporal correlations and scaling behavior in human brain oscillations. *Journal of*
 1486 *Neuroscience*, *21*(4), 1370–1377.
- 1487 Lopez da Silva, F. H. (2018). *Niedermeyer's Electroencephalography*. Oxford University
 1488 Press.
- 1489 Lundqvist, M., Rose, J., Herman, P., Brincat, S. L., Buschman, T. J., & Miller, E. K. (2016).
 1490 Gamma and Beta Bursts Underlie Working Memory. *Neuron*, *90*(1), 152–164.
 1491 <http://doi.org/10.1016/j.neuron.2016.02.028>
- 1492 Mierau, A., Klimesch, W., & Lefebvre, J. (2017). State-dependent alpha peak frequency
 1493 shifts: Experimental evidence, potential mechanisms and functional implications.
 1494 *Neuroscience*, *360*, 146–154. <http://doi.org/10.1016/j.neuroscience.2017.07.037>

- 1495 Molenaar, P. C. M., & Campbell, C. G. (2009). The new person-specific paradigm in
 1496 psychology. *Current Directions in Psychological Science*, *18*(2), 112–117.
 1497 <http://doi.org/10.1111/j.1467-8721.2009.01619.x>
- 1498 Muthukumaraswamy, S. D., & Singh, K. D. (2011). A cautionary note on the interpretation of
 1499 phase-locking estimates with concurrent changes in power. *Clinical Neurophysiology*,
 1500 *122*(11), 2324–2325. <http://doi.org/10.1016/j.clinph.2011.04.003>
- 1501 Nolan, H., Whelan, R., & Reilly, R. B. (2010). FASTER: Fully Automated Statistical
 1502 Thresholding for EEG artifact Rejection. *Journal of Neuroscience Methods*, *192*(1), 152–
 1503 162. <http://doi.org/10.1016/j.jneumeth.2010.07.015>
- 1504 Oldfield, R. C. (1971). The assessment and analysis of handedness: The Edinburgh inventory.
 1505 *Neuropsychologia*, *9*(1), 97–113. [http://doi.org/10.1016/0028-3932\(71\)90067-4](http://doi.org/10.1016/0028-3932(71)90067-4)
- 1506 Oostenveld, R., Fries, P., Maris, E., & Schoffelen, J. M. (2011). FieldTrip: Open source
 1507 software for advanced analysis of MEG, EEG, and invasive electrophysiological data.
 1508 *Computational Intelligence and Neuroscience*, *2011*(1), 156869–9.
 1509 <http://doi.org/10.1155/2011/156869>
- 1510 Perrin, F., Pernier, J., Bertrand, O., & Echallier, J. F. (1989). Spherical splines for scalp
 1511 potential and current density mapping. *Electroencephalography and Clinical*
 1512 *Neurophysiology*, *72*(2), 184–187.
- 1513 Peterson, E. J., & Voytek, B. (2017). Alpha oscillations control cortical gain by modulating
 1514 excitatory-inhibitory background activity. *bioRxiv*, 185074.
 1515 <http://doi.org/10.1101/185074>
- 1516 Raghavachari, S., Kahana, M. J., Rizzuto, D. S., Caplan, J. B., Kirschen, M. P., Bourgeois, B.,
 1517 et al. (2001). Gating of human theta oscillations by a working memory task. *Journal of*
 1518 *Neuroscience*, *21*(9), 3175–3183. <http://doi.org/10.1523/JNEUROSCI.21-09-03175.2001>
- 1519 Sadaghiani, S., & Kleinschmidt, A. (2016). Brain Networks and α -Oscillations: Structural and
 1520 Functional Foundations of Cognitive Control. *Trends in Cognitive Sciences*, *20*(11), 805–
 1521 817. <http://doi.org/10.1016/j.tics.2016.09.004>
- 1522 Samaha, J., & Postle, B. R. (2015). The Speed of Alpha-Band Oscillations Predicts the
 1523 Temporal Resolution of Visual Perception. *Current Biology*, *25*(22), 2985–2990.
 1524 <http://doi.org/10.1016/j.cub.2015.10.007>
- 1525 Sherman, M. A., Lee, S., Law, R., Haegens, S., Thorn, C. A., Hämäläinen, M. S., et al.
 1526 (2016). Neural mechanisms of transient neocortical beta rhythms: Converging evidence
 1527 from humans, computational modeling, monkeys, and mice. *Proceedings of the National*
 1528 *Academy of Sciences*, *113*(33), E4885–E4894. <http://doi.org/10.1073/pnas.1604135113>

- 1529 Shin, H., Law, R., Tsutsui, S., Moore, C. I., & Jones, S. R. (2017). The rate of transient beta
 1530 frequency events predicts behavior across tasks and species. *eLife*, 6.
 1531 <http://doi.org/10.7554/eLife.29086>
- 1532 Sternberg, S. (1966). High-speed scanning in human memory. *Science*, 153(3736), 652–654.
- 1533 Stokes, M., & Spaak, E. (2016). The Importance of Single-Trial Analyses in Cognitive
 1534 Neuroscience. *Trends in Cognitive Sciences*, 20(7), 483–486.
 1535 <http://doi.org/10.1016/j.tics.2016.05.008>
- 1536 Tinkhauser, G., Pogosyan, A., Tan, H., Herz, D. M., Kühn, A. A., & Brown, P. (2017). Beta
 1537 burst dynamics in Parkinson’s disease OFF and ON dopaminergic medication. *Brain*,
 1538 140(11), 2968–2981. <http://doi.org/10.1093/brain/awx252>
- 1539 Tuladhar, A. M., Huurne, ter, N., Schoffelen, J. M., Maris, E., Oostenveld, R., & Jensen, O.
 1540 (2007). Parieto-occipital sources account for the increase in alpha activity with working
 1541 memory load. *Human Brain Mapping*, 28(8), 785–792. <http://doi.org/10.1002/hbm.20306>
- 1542 van Ede, F., Quinn, A. J., Woolrich, M. W., & Nobre, A. C. (2018). Neural Oscillations:
 1543 Sustained Rhythms or Transient Burst- Events? *Trends in Neurosciences*, 1–3.
 1544 <http://doi.org/10.1016/j.tins.2018.04.004>
- 1545 Vidaurre, D., Myers, N., Stokes, M., Nobre, A. C., & Woolrich, M. W. (2018). Temporally
 1546 unconstrained decoding reveals consistent but time-varying stages of stimulus processing,
 1547 1–23. <http://doi.org/10.1101/260943>
- 1548 Vidaurre, D., Quinn, A. J., Baker, A. P., Dupret, D., Tejero-Cantero, A., & Woolrich, M. W.
 1549 (2016). Spectrally resolved fast transient brain states in electrophysiological data.
 1550 *NeuroImage*, 126(C), 81–95. <http://doi.org/10.1016/j.neuroimage.2015.11.047>
- 1551 Wang, X. J. (2010). Neurophysiological and Computational Principles of Cortical Rhythms in
 1552 Cognition. *Physiological Reviews*, 90(3), 1195–1268.
 1553 <http://doi.org/10.1152/physrev.00035.2008>
- 1554 Watrous, A. J., Miller, J., Qasim, S. E., Fried, I., & Jacobs, J. (2018). Phase-tuned neuronal
 1555 firing encodes human contextual representations for navigational goals. *eLife*, 7.
 1556 <http://doi.org/10.7554/eLife.32554>
- 1557 Westner, B. U., Dalal, S. S., Hanslmayr, S., & Staudigl, T. (2018). Across-subjects
 1558 classification of stimulus modality from human MEG high frequency activity. *PLoS*
 1559 *Computational Biology*, 14(3), e1005938. <http://doi.org/10.1371/journal.pcbi.1005938>
- 1560 Whitten, T. A., Hughes, A. M., Dickson, C. T., & Caplan, J. B. (2011). A better oscillation
 1561 detection method robustly extracts EEG rhythms across brain state changes: The human

- 1562 alpha rhythm as a test case. *NeuroImage*, 54(2), 860–874.
1563 <http://doi.org/10.1016/j.neuroimage.2010.08.064>
1564 Wutz, A., Melcher, D., & Samaha, J. (2018). Frequency modulation of neural oscillations
1565 according to visual task demands. *Proceedings of the National Academy of Sciences*,
1566 115(6), 1346–1351. <http://doi.org/10.1073/pnas.1713318115>
1567